SÃO PAULO STATE UNIVERSITY
FACULTY OF ENGINEERING OF BAURU
MECHANICAL ENGINEERING POST-GRADUATION PROGRAM

POSITIONING AND VIBRATION CONTROL OF A FLEXIBLE STRUCTURE IN SLEWING MOTION BY APPLYING SHAPE MEMORY ALLOYS

Author: Frederic Conrad Janzen
Advisor: Full Professor José Manoel Balthazar

Bauru, 2016
SP, Brazil

SÃO PAULO STATE UNIVERSITY
FACULTY OF ENGINEERING OF BAURU
MECHANICAL ENGINEERING POST-GRADUATION PROGRAM

POSITIONING AND VIBRATION CONTROL OF A FLEXIBLE STRUCTURE IN SLEWING MOTION BY APPLYING SHAPE MEMORY ALLOYS

Author: Frederic Conrad Janzen
Advisor: Full Professor José Manoel Balthazar

Course: Mechanical Engineering
Area of concentration: Mechanical Project

Ph.D. Dissertation to be presented to the Program of Post-Graduation in Mechanical Engineering of the Faculty of Engineering of Bauru - São Paulo State University, as one of the requirements for the degree of the Doctor of Philosophy in Mechanical Engineering.

Bauru, 2016
SP, Brazil

Janzen, Frederic Conrad.
Positionig and vibration control of a flexible structure in slewing motion by applying Shape Memory Alloys / Frederic Conrad Janzen, 2016
100 f. : il.

Orientador: José Manoel Balthazar

Tese (Doutorado)–Universidade Estadual Paulista. Faculdade de Ciências, Bauru, 2016

1. Slewing. 2. Flexible beam. 3. Active control. 4. Shape Memory Alloys I. Universidade Estadual Paulista. Faculdade de Ciências. II. Título.

UNIVERSIDADE ESTADUAL PAULISTA

Câmpus de Bauru

ATA DA DEFESA PÚBLICA DA TESE DE DOUTORADO DE FREDERIC CONRAD JANZEN, DISCENTE DO PROGRAMA DE PÓS-GRADUAÇÃO EM ENGENHARIA MECÂNICA, DA FACULDADE DE ENGENHARIA.

Aos 19 dias do mês de setembro do ano de 2016, às 09:00 horas, no(a) Anfiteatro do DTI, reuniu-se a Comissão Examinadora da Defesa Pública, composta pelos seguintes membros: Prof. Dr. JOSE MANOEL BALTHAZAR - Orientador(a) do(a) Departamento de Estatística, Matemática Aplicada e Computação / Instituto de Geociências e Ciências Exatas - UNESP Rio Claro, Prof. Dr. ANGELO MARCELO TUSSET do(a) Departamento de Eletrônica / Universidade Tecnológica Federal do Paraná, Prof. Dr. VINICIUS PICCIRILLO do(a) Departamento de Matemática/Universidade Tecnológica Federal do Paraná, Prof. Dr. AIRTON NABARRETE do(a) Departamento de Engenharia Aeroespacial e Aeronáutica / Instituto Tecnológico de Aeronáutica, Prof. Dr. ATILA MADUREIRA BUENO do(a) Departamento de Engenharia de Controle e Automação / Instituto de Ciência e Tecnologia/UNESP/Sorocaba, sob a presidência do primeiro, a fim de proceder a arguição pública da TESE DE DOUTORADO de FREDERIC CONRAD JANZEN, intitulada **POSITIONING AND VIBRATION CONTROL OF A FLEXIBLE STRUCTURE IN SLEWING MOTION BY APLLYING SHAPE MEMORY ALLOYS**. Após a exposição, o discente foi arguido oralmente pelos membros da Comissão Examinadora, tendo recebido o conceito final: APROVADO. Nada mais havendo, foi lavrada a presente ata, que após lida e aprovada, foi assinada pelos membros da Comissão Examinadora.

Prof. Dr. JOSE MANOEL BALTHAZAR

Prof. Dr. ANGELO MARCELO TUSSET

Prof. Dr. VINICIUS PICCIRILLO

Prof. Dr. AIRTON NABARRETE

Prof. Dr. ATILA MADUREIRA BUENO

Dedicated to

My wife Meri Elen and to my daughter Julia

Acknowledgements

In first and foremost thank God for being my strength and guide in the writing of this thesis. Without Him, I would not have had the ability to do so.

I extend the warmest and heartfelt thanks to my advisor, Professor Dr. José Manoel Balthazar, for his inspiration, enthusiasm and friendship.

My sincere thanks also goes to Dr. Angelo Marcelo Tusset for their insightful comments and encouragement and for his friendship.

Last but not the least, I would like to thank my family: my wife and to my daughter for supporting me throughout writing this thesis.

Acknowledgements for CNPq for the financial support: "Processo:447539/2014-0. Edital: Apoio a Projetos de Pesquisa / MCTI/CNPQ/Universal 14/2014".

Resumo

Janzen, F. C., CONTROLE DO POSICIONAMENTO E VIBRAÇÃO DE UMA ESTRUTURA FLEXIVEL EM MOVIMENTO DE GIRO COM APLICAÇÃO DE LIGAS COM MEMÓRIA DE FORMA, Bauru, Faculdade de Engenharia, UNESP – Universidade Estadual Paulista, 2016, 100 p., Tese de Doutorado.

Estruturas flexíveis com movimento de rastreamento tem sido encontradas com frequência cada vez maior em diversos tipos de aplicações, por serem mais eficientes do que suas concorrentes rígidas. O estudo desses sistemas é importante por conta das vibrações advindas da redução de massa das estruturas. Muitos trabalhos têm sido publicados apresentado técnicas de controle aplicadas na redução dos efeitos dessas vibrações. Vários trabalhos demonstram a aplicação de materiais inteligentes como atuadores para esse tipo de aplicação. Sendo assim, o presente trabalho apresenta uma proposta para o controle do posicionamento angular e da vibração de uma estrutura flexível em movimento de rastreamento. Para tal, atuadores compostos de um material inteligente conhecido como Liga com Memoria de Forma são empregados para o controle da vibração da estrutura flexível. Com relação ao controle, a técnica de controle conhecida como Equações de Ricatti Dependentes dos Estados (SDRE) é aplicada para o controle. Com o objetivo de analisar a dinâmica do sistema com o controle proposto considera-se a modelagem matemática do sistema e sua validação através do desenvolvido de um protótipo experimental. Simulações numéricas são realizadas para analisar a viabilidade do controle proposto e testes experimentais são realizados com a finalidade de validar o modelo teórico e a proposta de controle.

Palavras-chave: Movimento de Giro, Vigas flexível, Controle ativo, Ligas com Memoria de Forma

Abstract

Janzen, F. C., POSITIONING AND VIBRATION CONTROL OF A FLEXIBLE STRUCTURE IN SLEWING MOTION BY APPLYING SHAPE MEMORY ALLOYS , Bauru, Faculty of Engineering, São Paulo State University, 2016, 100 p., Ph.D. Dissertation.

Flexible structures with slewing motion has been found with increasing frequency in various types of applications, because they are more efficient than their rigid competitors. The study of these systems is important because of the vibrations coming from the mass reduction of structures. Many works have been published presenting control techniques applied in reducing the effects of these vibrations. Several studies demonstrate the application of intelligent materials as actuators for this application. This paper presents a proposal for controlling the angular positioning and vibration of a flexible structure in slewing motion. For such compounds an intelligent actuator materials known as Shape Memory Alloy is employed to control the vibration of the flexible structure. To control the system, the control technique known as State Dependent Ricatti Equation (SDRE), is applied to the control. In order to analyse the dynamics of the system with the proposed control the mathematical modelling of the system is considered and its validation by developed an experimental prototype. Numerical simulations are carried out to analyse the viability of the control and experimental tests are performed in order to validate the theoretical model and the proposed control.

Keywords:Slewing, Flexible beam, Active control, Shape Memory Alloys

List of Figures

List of Tables

Contents

Nomenclature

Latin Letter

Symbols	Description
A	Beam cross section area
A_f	Austenite final temperature
A_s	Austenite start temperature
A_{SMA}	Shape Memory Alloy cross section area
b	Viscous friction
C_A	Effect of stress on austenite temperature
C_M	Effect of stress on martensite temperature
C_ρ	SMA specific heat
E	Beam Young modulus
e	Counter electromotive force
E_A	Shape Memory Alloy Austenite Young modulus
E_M	Shape Memory Alloy Martensite Young modulus
h	Heat convection coefficient
I	Beam cross section moment of inertia
i_a	Armature Current
J	Moment of inertia
K_b	Counter electromotive force constant
K_t	Torque constant
L	Beam Length
L_m	Armature Inductance

M_f	Martensite final temperature
M_s	Martensite start temperature
n	Beam vibration mode number
R	Armature Resistance
R_{SMA}	SMA resistance
T_{in}	Ambient temperature
V	Armature Voltage

Greek Letter

Symbols	**Description**
ε	SMA strain
ε_0	Initial strain
ϕ_n	Beam vibration mode shape
μ	Structural damping coefficient
ν	Beam displacement
θ	Angular position
Θ	Thermal expansion factor
$\dot{\theta}$	Angular speed
$\tilde{\theta}$	Total angular position
ρ	Beam material density
σ	SMA stress
σ_{in}	Initial SMA stress
τ	Torque
ω_n	Beam natural frequency
ξ	Martensitic fraction

Abbreviation

Symbol	**Description**
DAQ	Data Acquisition
DC	Direct Current
FBG	Fiber Bragg Grating
LQR	Linear Quadratic Regulator
PWM	Pulse Width Modulation
SMA	Shape Memory Alloy
$SDRE$	State Dependent Ricatti Equation
$SSRMS$	Space Station Remote Manipulator System
PZT	Lead Zirconate Titanate

Chapter 1

Introduction

In some kinds of applications like in aerospace systems, the usage of rigid structures in the most cases is not economically viable. In these systems, the mass and the large working area are critical factors to be considered in the project.

In these cases, normally the best solution is the application of long and lightweight structures. This kind of structures have the characteristic to be flexible, what brings a big challenge to the control and stability of these systems. The flexibility makes these structures vibrate in lager amplitudes, what reduces the precision and dexterity of the system and in some cases can broke or destroy the system.

In the some of the cases, the flexible structures are working in slewing motions. Slewing structures are they what moves about a fixed point. Some examples of the application of this kind of structures are a link of a robotic manipulator, an appendage of a satellite, antennas, and some others (Garcia and Inman, 1990a).

An example of some kind of system with flexible structures is the Space Station Remote Manipulator System, or SSRMS, presented in Fig. 1.1. This system is a robotic manipulator with 17.6 m long, divided in 7 degrees of freedom. In order to make it be possible to transport the SSRMS to the Space Station the same had to be designed lightweight as possible in comparison whit robotic manipulators that works on the earth (Tokhi and Azad, 2008; Stieber et al., 1999)

Another important requisite to be considered is the energy efficiency of this kind of systems. Not just for the aerospace systems which have limited power source consisting by battery's and solar panels, but for industrial applications to. The demand for more efficient systems increase every time. The lighter the structure of a robotic manipulator for example, the lower need to be the actuator, and consequently lower is the power needed to torque drive the system.

To make it possible the use of flexible structures in slewing systems, the influence of the flexibility over the system and its control need to be understood. In this way, many

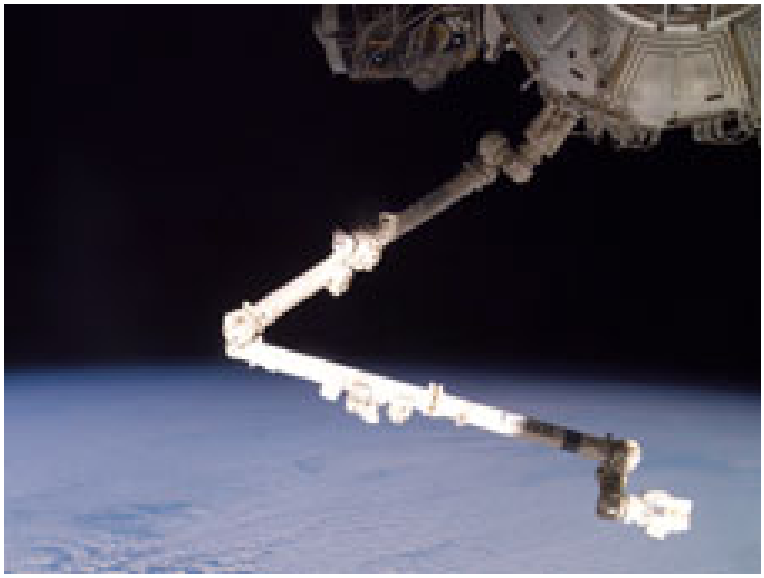

Figure 1.1: Space Station Remote Manipulator System (SSRMS)(NASA, 2015).

works have been developed in order to analyse the dynamic behaviour of this systems and to propose ways to control the systems and minimize the effects of the vibration. Between this are the works presented by Tokhi and Azad (1996), Stieber et al. (1999), Fenili et al. (2003), Garcia and Inman (1990b),Janzen et al. (2014a) and Ge et al. (2006).

According to Tokhi and Azad (1996), two factors that difficult the control of flexible slewing systems are: the control torque can be applied just to the joints of the system, and just a limited number of sensors can be applied to the flexible structure.

By considering this, some works have been developed in order to suppress the vibrations of flexible structures reducing the negative effects of the flexibility over the system control. In his work, Garcia and Inman (1990a) proposes an active control of the vibrations of a flexible structure in slewing motions by applying piezoelectric (PZT) actuators to the structure. This kind of actuators are considered as intelligent materials.

Other kinds of intelligent materials have been applied in order to suppress vibrations in flexible structures like electrorheological and magnetorheological fluids and Shape Memory Alloys (SMA)(Sohn et al., 2009).

Janzen et al. (2014a) and Ge et al. (2006), presents in is works the application of SMA actuators coupled to flexible structures in order to control and suppress the vibrations caused by a slewing motion.

According to Wei et al. (1998), the SMA actuators have a high damping capacity and to change the natural vibration modes of the structures where they are coupled.

Several control techniques have been applied to control alloy actuators shape memory, as classic control techniques with PID and its variants presented in Ge et al. (2006), and

non-linear controllers as shown by Elahinia (2004). In his work Janzen et al. (2014a) showed the use of a non-linear control known as SDRE (Dependent state Ricatti Equations) to control both the positioning of the vibration as a flexible tracking system using SMA actuators .

1.1 Objectives

The main objective of this work is to control of the angular position of the end point of a slewing flexible structure by suppressing its flexural deflections (vibrations) by applying Shape Memory Alloys actuators to the structure, improving the system settling time.

Specifically, we intend to:

1. Apply the mathematical models for the slewing system and SMA actuators.
2. Provide models to couple the actuator to the flexible structure.
3. Conduct numerical simulations in order to analyze the system dynamics.
4. Develop experimental the experimental system.

1.2 Approach

The approach adopted in this research will include a literature review to provide a summary of the models that will be developed. Next, we will develop the dynamic models for each component of the system separately. Numerical simulations will be performed for all the system components. The numerical simulations are reproduced experimentally in order to validate the dynamic mathematical models.

After, the models will be coupled in order to represent the flexible structure slewing system with vibration control trough SMA actuators. Numerical simulations will be performed. The experimental system is developed and the experimental and numerical results will be analyzed.

1.3 Thesis Outline

Chapter 1 concludes with the outlines of this study. Chapter 2, presents the description and modelling of the system in study. A complete description of the system is presented in section 2.1. The mathematical model for a DC motor is described in section 2.2. Section 2.3 presents the modelling of a flexible beam like structure. The coupling between motor and structure are discussed in section 2.4. The control technique which controls the angular positioning is presented in section 2.5 and its design is made in section 2.5.1. Numerical simulation results and experimental results are analysed and discussed in section 2.6.

In Chapter 3, an SMA phenomenological model is presented and analysed. Section 3.1 and 3.2 presents a brief literature review. In section 3.3, the SMA model used in this thesis is presented and described. Numerical simulations of the SMA model are presented in section 3.4. Section 3.5, presents the experimental set-up used to characterize a SMA actuator. The experimental results are presented, analysed and compared in section 3.6.

The Chapter 4, is intended to describe and analyse the coupling model between the SMA actuator and the flexible structure. Section 4.1 presents the proposed coupling model. In section 4.2, numerical simulations are presented in order to analyse the proposed model. Where section 4.2.1 presents the results for the system without the SMA actuation, just angular positioning control, and section 4.2.2 the results for the system with the SMA actuation, positioning and vibration control.

In Chapter 5, the experimental set-up development and the experimental results are presented. Section 5.1 is dedicated to describe the experimental set-up. In section 5.2, the development of the DC motor drive is presented. The experimental results for the angular positioning control are presented and analysed in section 5.3. Section 5.4 is intended to present and analyse the experimental results for the system with the vibration control.

Finally the Appendix A, presents the methodology applied to characterize the DC motor parameters.

Chapter 2

Flexible Slewing System Model

In this chapter, the flexible slewing structure system is described, modeled and analyzed.

The complete system will be modeled and analyzed in parts. All the components of the system will be presented separately and its models will be presented and analyzed through numerical simulations and experimental test. The SDRE control technique will be presented and designed for the angular position control.

2.1 System Description

The slewing system studied in this thesis, Fig. 2.1, is composed by a DC motor controlled through the armature current, and by a flexible beam like structure, which is coupled to the DC motor shaft.

In figure 2.1, θ represents the angular position of the motor shaft. Considering that the flexible beam like structure and the DC motor shaft are mechanically coupled, the angular position of the clamped end of the structure and the DC motor shaft are the same. Tacking account the flexibility of the beam like structure, his free end can vibrate in the flexural mode when the DC motor angular position is controlled. This vibration displacement is represented by ν in Fig. 2.1. This thesis considers just the first flexural vibration mode of the flexible beam like structure. The other vibration modes and the torsional vibrations are neglected.

The angular position can assume any value between 0 and 2π radians, but for standardization will be discussed only shifts between 0 and 1 radians. The displacement of the free end of the beam due to vibration is considered small relative to the angular displacement of the fixed end. Thus, it is possible to consider the total angular position of the free end of the beam as the sum of the motor angle and displacement of the free end as showed in

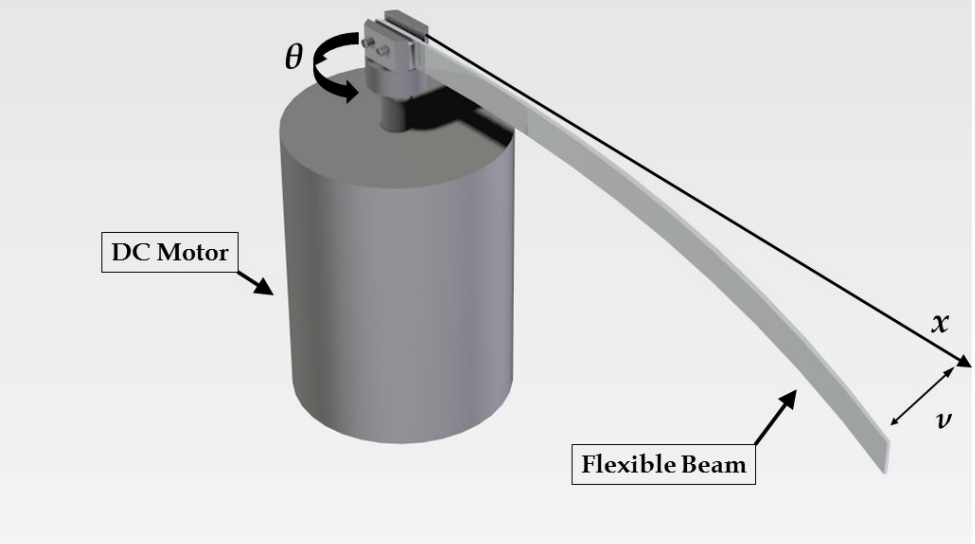

Figure 2.1: Schematic drawing of the studied system, composed by a flexible beam like structure coupled to a DC motor shaft.

Eq. (2.1) (Garcia and Inman, 1990b; Tokhi and Azad, 2008).

$$\tilde{\theta} = \theta + \nu \tag{2.1}$$

The system dynamics is considered as non ideal, it means that the dynamic equations takes account the energy change between DC motor and flexible structure. The DC motor torque drives the flexible structure when fired. In the same mode, the vibrations of the flexible structure caused by this movement are couple to the DC motor.

The main objective of the system is to control the angular position of the system. The big challenge involved in this control is the flexibility of the beam like structure. The flexibility need to be considered in the control project to have a bather performance of the positioning controller.

In this chapter, the slewing system will be modeled. Firstly the section 2.2 the dynamic equations of the DC motor are obtained. In Sec. 2.3 the flexible beam like structure is modeled and his equations of motion are obtained. Section 2.4 present the coupling of the flexible structure and the DC motor. Section 2.5 presents the proposed control technique for the positioning control. In Sec. 2.6 presents numerical simulation results of the slewing system and some analysis. Finally, in section 2.6 experimental results are presented in order to validate the proposed model.

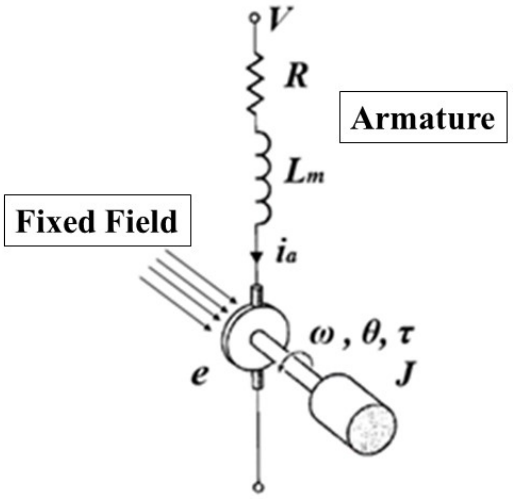

Figure 2.2: Schematic drawing of a DC motor controlled through the armature current.

2.2 DC Motor Model

The DC motor is an actuator that converts continuous electric current to rotating mechanical power, known as torque (Dorf and Bishop, 2001). There are several types of DC motors, and in this thesis, the DC motor type used is the fixed field or permanent magnet as shown in Fig. 2.2. This type of motor is often used because of its ease control speed and angular position control. The control of these motors is achieved by controlling the voltage applied to the motor armature.

Considering that the magnetic field generated by the permanent magnet is fixed, it is possible to write the torque generated by the engine as being proportional to the armature current, i_a, multiplied by a torque constant K_t as shown in Eq. (2.2).

$$\tau = K_t i_a \tag{2.2}$$

The counter electromotive force generated by the motor, which is represented by e in Fig.2.2, can be described as proportional to the angular speed of the motor shaft *omega*, multiplied by an electromotive force constant K_b as showed in Eq. (2.3).

$$e = K_b \dot{\theta} \tag{2.3}$$

By applying the Newton's second law to the mechanical system in Fig. 2.2, the equation of motion of the mechanical system of the DC motor is obtained as presented in Eq.(2.4).

$$J\ddot{\theta} + b\dot{\theta} = K_t i_a \tag{2.4}$$

Where b is the viscous friction from the moving parts of the motor. J represents the sum of the moments of inertia from the beam like structure, motor shaft and the beam shaft coupling hub and i_a.represents the electric current applied to the armature.

Applying the Kirchhoff's voltage law to the electric system in Fig. 2.2, equation (2.5) is obtained, that represents the behaviour of the electric system of the motor.

$$L_m \frac{di_a}{dt} + Ri_a = V - K_b\dot{\theta} \tag{2.5}$$

where L_m and R are the armature inductance and resistance respectively.

Equations (2.4) and (2.5) together represents the DC motor equations of motion. The both equations are coupled through the electric current and angular speed.

The simulation parameters for the DC motor is obtained by measuring experimentally the DC motor the DC motor applied in the experimental set-up. The methodology applied to obtain these parameters is presented in Appendix A.

2.3 Flexible Beam Like Structure Model

In this thesis, the slewing beam like structure is modelled as a fixed-free cantilever beam. The fixed end is connected directly to the motor shaft. To obtain the equations of motion it is considered that the beam follows the Euler-Bernoulli beam theory.

Figure 2.3 presents de motion of the slewing structure, where X and Y are the fixed reference frame, and x and y represents the rotating reference frame (Garcia and Inman, 1990b). This rotating frame represents the position of undelflected beam like structure. In Fig. 2.3 θ represents the angular displacement of the undelflected structure and L the beam length.

The position of any point over the flexible structure in relation to the X,Y reference frame can be defined through the vector R as showed in Eq. (2.6).

$$\vec{R} = \left(x\cos\left(\theta\right) - v\sin\left(\theta\right)\right) i + \left(x\sin\left(\theta\right) + \nu\cos\left(\theta\right)\right) j \tag{2.6}$$

In this model, any point of the flexible beam like structure is free to move parallel to the y frame where the displacement is represented by ν. For small displacements in the y direction, the displacement in the longitudinal, or x direction can be neglected (Fenili, 2000). This thesis do not consider displacements in the x direction.

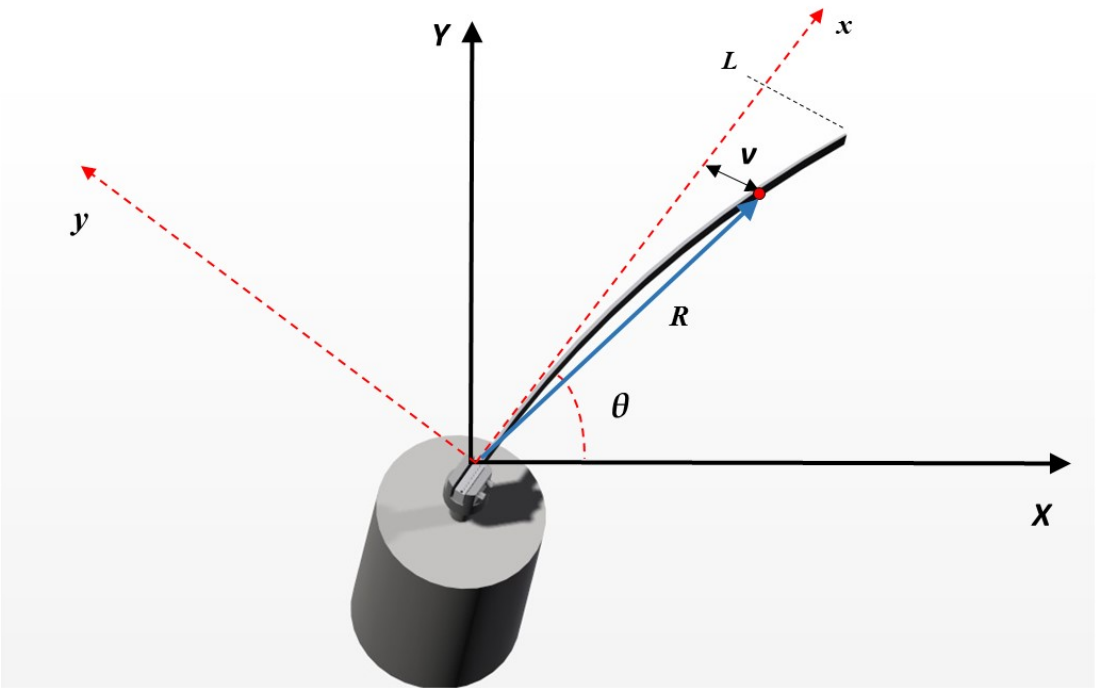

Figure 2.3: Schematic draw of the beam like structure rotating motion.

To obtain the kinetic energy of the beam like structure it is necessary to obtain the square of its speed. The speed can be described as showed in Eq. (2.7).

$$\begin{aligned}\vec{R} = &\left(\dot{x}\cos(\theta) - xsin\left(\theta\dot{\theta}\right) - \nu cos\left(\theta\dot{\theta}\right) - \dot{v}\sin(\theta)\right)i + \\ &+\left(\dot{x}\sin(\theta) + xcos\left(\theta\dot{\theta}\right) + \dot{\nu}cos(\theta) - \nu\sin\left(\theta\dot{\theta}\right)\right)j\end{aligned} \tag{2.7}$$

By evaluating the square of Eq. (2.7) and considering that x=0 , it means, there are not displacements in the x direction, Eq. (2.8) is obtained.

$$\left|\dot{\vec{R}}\right|^2 = \left(\dot{\nu} + x\dot{\theta}\right)^2 + \left(\dot{x} - \nu\dot{\theta}\right)^2 \tag{2.8}$$

The kinetic energy can now written as showed in Eq. (2.9) (Garcia and Inman, 1990b).

$$T = \frac{1}{2}\rho A\int_0^L \left(\dot{\nu} + x\dot{\theta}\right)^2 + \left(\nu\dot{\theta}\right)^2 dx \tag{2.9}$$

In equation (2.9) ρ is the material density and A is the cross section area of the beam like structure.

The potential elastic energy of the flexible structure is obtained from Garcia and Inman

(1990b), and can be written as:

$$V = \frac{1}{2}\int_0^L EI\,(\nu'')^2 dx \tag{2.10}$$

In equation (2.10) E is the Young's modulus of the beam like structure material and I is his area momentum of inertia.

The Lagrangian of the flexible structure in a slewing motion can be expressed as:

$$L_g = \frac{1}{2}\rho A \int_0^L \left(\dot{\nu} + x\dot{\theta}\right)^2 + \left(\nu\dot{\theta}\right)^2 dx - \frac{1}{2}\int_0^L EI\,(\nu'')^2 dx \tag{2.11}$$

The non-conservative work done by the applied torque from the DC motor can be written as presented in Eq. (2.12).

$$W_{nc} = \tau\tilde{\theta} \tag{2.12}$$

To obtain the equations of motion of the slewing structure, the extended Hamilton's principle is applied. This is an energy method described in Gantmakher (1970) and Meirovitch (1967). The Hamilton's principle considers the motion of the system between two times t_1 and t_2 reducing the problem to a scalar definite integral (Meirovitch, 1967).

The extended Hamilton's principle can be written as:

$$\delta \int_{t_1}^{t_2} (L_g + W_{nc})dt = 0 \tag{2.13}$$

where $\delta(t_1\ )$=$\delta(t_2\ )$= 0.

Substituting the Lagrangian Eq. (2.11) and the non-conservative work Eq. (2.12) into the extended Hamilton's principle Eq. (2.13) the following equation is obtained:

$$\delta \int_{t_1}^{t_2} \left\{ \frac{1}{2}\rho A \int_0^L \left[\left(\dot{\nu} + x\dot{\theta}\right)^2 + \left(\nu\dot{\theta}\right)^2 \right] dx - \frac{1}{2}\int_0^L \left[EI(\nu'')^2 \right] dx + \tau\tilde{\theta} \right\} dt = 0 \tag{2.14}$$

To solve Eq. (2.14) it is needed to derive them in relation to his variables, obtaining so Eq. (2.15).

$$\int_{t_1}^{t_2} \left(\frac{\partial L_g}{\partial \dot{\theta}}\delta\dot{\theta} + \frac{\partial L_g}{\partial \dot{\nu}}\delta\dot{\nu} + \frac{\partial L_g}{\partial x}\delta x + \frac{\partial L_g}{\partial \nu}\delta\nu + \frac{\partial L_g}{\partial \nu''}\delta\nu'' + \frac{\partial L_g}{\partial \tilde{\theta}}\delta\tilde{\theta} \right) dt = 0 \tag{2.15}$$

By solving Eq. (2.15), we obtain Eq. (2.16).

$$\int_{t_1}^{t_2} \left\{ \begin{array}{l} \rho A \int_0^L \left[\left(\dot{\theta}\nu^2 + \dot{\theta}x^2 + \dot{\nu}x \right) \delta\dot{\theta} + \left(\dot{\theta}x + \dot{\nu} \right) \delta\nu + \left(\dot{\nu}\dot{\theta} + x\dot{\theta}^2 \right) \delta x + \left(\dot{\theta}^2\nu \right) \right] dx - \\ -EI \int_0^L \left[\left(\nu'' \right) \delta\nu'' \right] dx + \tau\tilde{\theta} \end{array} \right\} dt = 0 \tag{2.16}$$

Integrating by parts, the terms multiplied by $\delta\dot{\theta}$, $\delta\dot{\nu}$, $\delta\nu''$ in Eq. (2.16) and separating the contour terms it is possible to obtain:

$$\int_{t_1}^{t_2} \left\{ \begin{array}{ll} \rho A \int_0^L & \left[\left(-\ddot{\theta}\nu^2 - 2\dot{\theta}\nu\dot{\nu} - \ddot{\theta}x^2 - \ddot{\nu}x \right) \right] \delta\theta dx + \\ & + \rho A \int_0^L \left[\left(\dot{\theta}^2\nu - \ddot{\theta}x - \ddot{\nu} \right) - EI\nu^{IV} \right] \delta\nu dx + \tau\tilde{\theta} \end{array} \right\} dt = 0 \tag{2.17}$$

with the contour terms:

$$\int_0^L \left\{ \left[\rho A \left(\dot{\theta}x + \dot{\nu} \right) \right] \delta\nu |_{t_1}^{t_2} \right\} dt \tag{2.18}$$

$$\int_{t_1}^{t_2} \left\{ \left[\left(EI\nu''' \right) \right] \delta\nu |_0^L \right\} dt \tag{2.19}$$

$$\int_0^L \left\{ \left[\rho A \left(\dot{\theta}\nu^2 + \dot{\theta}x^2 + \dot{\nu}x \right) \right] \delta\theta |_{t_1}^{t_2} \right\} dt \tag{2.20}$$

$$\int_{t_1}^{t_2} \left\{ \left[\left(EI\nu'' \right) \right] \delta\nu' |_0^L \right\} dt \tag{2.21}$$

The terms which depend on δx in Eq. (2.16) are eliminated because there is no variation in this parameter. According to the Hamilton's principle, $\delta\theta$ and $\delta\nu$ are null in time t_1 and t_2, and considering that by the clamped end of the beam like structure $\delta\nu(0,t) = 0$ and $\delta\nu''(0,t) = 0$ the equations of motion and the contour terms can be rewritten as:

$$\int_0^L \left\{ \rho A \left[\left(\ddot{\theta}\nu^2 + 2\dot{\theta}\nu\dot{\nu} + \ddot{\theta}x^2 + \ddot{\nu}x \right) \right] \right\} dx = \tau \tag{2.22}$$

$$\rho A \left(\dot{\theta}^2\nu - \ddot{\theta}x - \ddot{\nu} \right) - EI\nu^{IV} = 0 \tag{2.23}$$

with the contour terms:

$$\nu\left(0,t\right) = 0 \tag{2.24}$$

$$\nu'(0,t) = 0 \tag{2.25}$$

$$EI\nu''(L,t) = 0 \tag{2.26}$$

$$EI\nu'''(L,t) = 0 \tag{2.27}$$

Equation (2.22) represents the not deflected beam slewing motion and Eq. (2.23) is associated with the displacement in the y direction, or in other words with the motion caused due the flexibility.

2.3.1 Equations of Motion Discretization

The equations of motion of the slewing system Eq. (2.22) and Eq. (2.23) in section 2.3 are representing a system of infinite degrees of freedom. To solve this problem and discretize this equation, the Ritz method, or assumed modes method is applied to the equations of motion. After applying this method the system can be considered as composed of n degrees of freedom, where n represents the number of vibration modes.

The variable what represents the displacement due the flexibility can be discretized as showed in Eq. (2.28).

$$\nu(x,t) = \sum_{i=1}^{n} \phi_i(x) q_i(t) \tag{2.28}$$

where ϕ_i represents the mode shape and the variable q_i is the variable which will be determined.

Substituting Eq. (2.28) into Eq. (2.23), which represents the transversal deflection of the flexible structure Eq. (2.29) is obtained.

$$\rho A\dot{\theta}^2 \sum_{i=1}^{n} \phi_i q_i - \rho\ddot{\theta}x - \rho \sum_{i=1}^{n} \phi_i \ddot{q}_i - EI \sum_{i=1}^{n} {\phi_i}^{IV} q_i = 0 \tag{2.29}$$

In order to decouple the spatial variables, Eq. (2.29) is multiplied by an orthogonal eigenvector ϕ_l resulting in:

$$\rho A\dot{\theta}^2 \sum_{i=1}^{n} \phi_i \phi_l q_i - \rho\ddot{\theta}\phi_l x - \rho \sum_{i=1}^{n} \phi_i \phi_l \ddot{q}_i - EI \sum_{i=1}^{n} {\phi_i}^{IV} \phi_l q_i = 0 \tag{2.30}$$

Integrating Eq. (2.30) from $x = 0$ to $x = L$ and considering that $\int_0^L \phi_i \phi_l dx = 1$ if $i = l$ and $\int_0^L \phi_i \phi_l dx = 0$ if $i \neq l$ the following discretized equation of motion for the flexible

beam is obtained:

$$\ddot{q}_l + {\omega_l}^2 q_l + \alpha_l \ddot{\theta} - \dot{\theta}^2 q_l = 0 \tag{2.31}$$

where α_l is described as:

$$\alpha_l = \int_0^L x\phi_l dx \tag{2.32}$$

Equation (2.31) represents the equation of motion for the flexural displacement of the flexible beam like structure. This equation can now be solved easily by numeric integration algorithms.

The mode shapes ϕ, are described by Eq. (2.33).

$$\phi_n(x) = C_n\left[\cos(a_i x) - \cosh(a_i x) + \kappa_n\left(\sin(a_i x) + \sinh(a_i x)\right) + \gamma_n\left(\sin(a_i x) - \sinh(a_i x)\right)\right] \tag{2.33}$$

where C_n is a normalization constant, κ_n, γ_n and a_i are described as:

$$\kappa_n = \frac{\rho L^3}{(a_i L)^3 J} \tag{2.34}$$

$$\gamma_n = \frac{\sin(a_i L) - \sinh(a_i L) + \kappa_n\left(\cosh(a_i L) - \cos(a_i L)\right)}{\cos(a_i L) + \cosh(a_i L)} \tag{2.35}$$

$$\omega_n = (a_i L)^2 \sqrt{\frac{EI}{\rho L^4}} \tag{2.36}$$

where ω_n is natural frequency of the n^{th} vibration mode.

2.4 Beam like Structure and DC Motor Coupling

The coupling between the beam like flexible structure and the DC motor is made in order to analyses the energy exchange between both. The DC motor torque drives the beam like structure moving it in a slewing motion. The vibrations due to the flexibility are coupled to the motor shaft making it oscillate. This kind of system is called as a non ideal system.

Equation (2.31) already considers the effects due the DC motor rotation, now it is necessary to consider de effects of the beam over the motor shaft. This is made through considering the bending moment at the fixed end of the beam like structure, which can be

described as presented in Eq. (2.37).

$$M = EI\nu'' \tag{2.37}$$

In order to allow the coupling of Eq. (2.37) to the system equations of motion, they need to be discretized resulting in:

$$M = EI \sum_{i=1}^{n} \phi_i{}''(0)\, q_i \tag{2.38}$$

The bending moment is coupled to the DC motor shaft, which can be described as the subtraction of the bending moment from the DC motor torque.

The complete equations of motion of the proposed slewing system can be described based on equations (2.4), (2.5), (2.31) and (2.34), as presented in Eq. (2.39) to Eq. (2.41). A dissipative force called as structural damping coefficient (μ) can be added to equation Eq. (2.31) which represents the damping effect of the beam like structure due to the friction (Fenili, 2000).

$$\frac{di_a}{dt} = -\frac{Ri_a}{L_m} + \frac{V}{L_m} - \frac{K_b\dot{\theta}}{L_m} \tag{2.39}$$

$$\ddot{\theta} = -\frac{b\dot{\theta}}{J} + \frac{K_t i_a}{J} - \frac{EI \sum_{i=1}^{n} \phi_i{}''(0)\, q_i}{J} \tag{2.40}$$

$$\ddot{q_l} = -\mu\dot{q_l} - {\omega_l}^2 q_l + \alpha_l\ddot{\theta} - \dot{\theta}^2 q_l \tag{2.41}$$

2.5 Angular Positioning Controller

The control of the angular position of the systems is proposed to be through the State Dependent Ricatti Equation (SDRE) control method. According to Mracek and Cloutier (1998), the SDRE is a suboptimal control which searches for the local stability of the system. One advantage of this method is that it obtain a closed loop solution which is locally asymptotically stable. Other advantage is that the method do not need the linearisation of the system, therefore not cancelling the benefits provided from the non-linearity's of the dynamic system (Molter et al., 2011; Fenili and Balthazar, 2005; Tusset et al., 2012).

The SDRE controller is projected to find a function u which is able to execute the positioning starting from an initial position, which is indicated by Eq. (2.42), to the

desired angular position indicated in Eq. (2.43)).

$$x\left(0\right) = x_0 \tag{2.42}$$

$$x\left(\infty\right) = x^* \tag{2.43}$$

where $x = \left[\begin{array}{ccccc} x_1 & x_2 & x_3 & x_4 & x_5 \end{array} \right]^T$ are the states, and x^* is the desired state.

According to Molter et al. (2011), the dynamic equations of the system can be rewritten as a first order equation in the form of state coefficient matrices as presented in Eq. (2.44).

$$\dot{x} = A\left(x\right)x + Bu \tag{2.44}$$

The quadratic cost function for the system is presented in Eq. (2.45).

$$J = \frac{1}{2}\int_{t_0}^{\infty} \left[e^T Q\left(x\right)e + u^T R\left(x\right)u\right]dt \tag{2.45}$$

In Eq. (2.45), the $Q(x)$ and $R(x)$ matrices are positive definite and represents the weights for the control outputs and inputs respectively.

The feedback control for each state is given by Eq. (2.46).

$$u = -R^{-1}\left(x\right)B^T\left(x\right)P\left(x\right)e \tag{2.46}$$

where the state dependent of the Ricatti equation to find $P(x)$ is given as by Eq. (2.47).

$$A^T\left(x\right)P\left(x\right) + P\left(x\right)A\left(x\right) - P\left(x\right)B\left(x\right)R^{-1}\left(x\right)B^T\left(x\right)P\left(x\right) + Q\left(x\right) = 0 \tag{2.47}$$

For each calculation of the u control, it is necessary to verify the system controllability by comparing if the rank of the matrix M Eq. (2.48) is equal to n.

$$M = \left[\begin{array}{cccc} B & A_{n\times n}B & ... & A^n_{n\times n}B \end{array} \right] \tag{2.48}$$

The SDRE controller can be defined by the following six steps algorithm:

- **Step 1:** Write the system in the form of Eq. (2.44).
- **Step 2:** Verify if the matrix Rank is equal to n.
- **Step 3:** Define $Q(x)$ and $R(x)$.
- **Step 4:** Solve Eq. (2.47) for each state.

- **Step 5:** Calculate the control signal u Eq. (2.46).
- **Step 6:** Integrate Eq. (2.44) and actualize each state.

A schematic illustration of this algorithm is presented in Fig. 2.4.

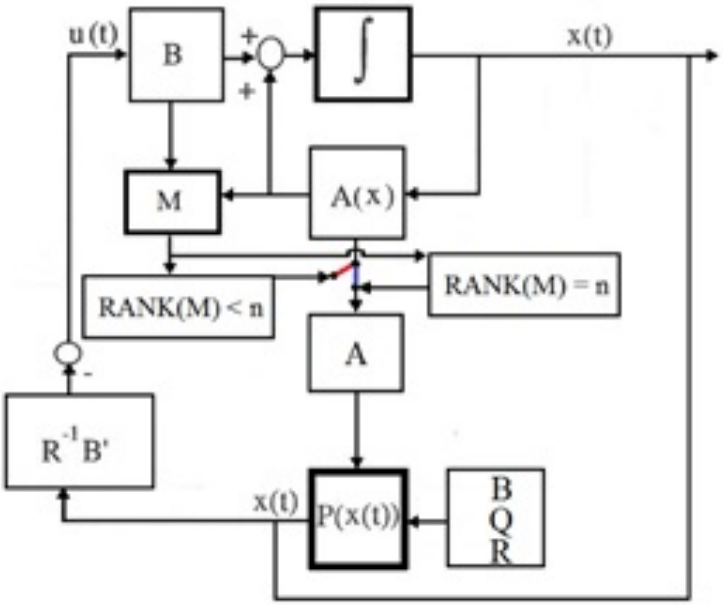

Figure 2.4: Bloc diagram of the SDRE controller (Janzen et al., 2014a).

2.5.1 Angular positioning Control Design

Following the presented SDRE algorithm, the first step is rewriting the equations of motion of the system presented in Eq. (2.39) to (2.41), in the form of Eq. (2.44). To do this, firstly, the system need to be written in the space state form as presented in Eq. (2.49).

$$\begin{aligned}
\dot{x}_1 &= -\frac{R}{L_m}x_1 + \frac{u}{L_m} - \frac{K_b}{L_m}x_3 \\
\dot{x}_2 &= x_3 \\
\dot{x}_3 &= -\frac{b}{J}x_3 + \frac{K_t}{J}x_1 - \frac{EI\sum_{i=1}^{n}\phi_i''(0)\,x_4}{J} \\
\dot{x}_4 &= x_5 \\
\dot{x}_5 &= -\mu x_5 - {\omega_l}^2 x_4 + \alpha_l \dot{x}_3 - {x_3}^2 x_4
\end{aligned} \tag{2.49}$$

where: $x_1 = i_a$, $x_2 = \tilde{\theta}$, $x_3 = \dot{\theta}$, $x_4 = q$, $x_5 = \dot{\theta}$ and u represents the control signal.

The system in Eq. (2.49) can be rewritten in the form of Eq. (2.44) as follows:

$$A(x) = \begin{bmatrix} -\frac{R}{L_m} & 0 & -\frac{K_b}{L_m} & 0 & 0 \\ 0 & 0 & 1 & 0 & 0 \\ \frac{K_t}{J} & 0 & -\frac{b}{J} & \frac{M}{J} & 0 \\ 0 & 0 & 0 & 0 & 1 \\ -\alpha\frac{K_t}{J} & 0 & \alpha\frac{b}{J} & \left(-{\omega_l}^2 - \alpha\frac{M}{J} + {x_3}^2\right) & -\mu \end{bmatrix} \tag{2.50}$$

$$B = \begin{bmatrix} \frac{1}{L_m} \\ 0 \\ 0 \\ 0 \\ 0 \end{bmatrix} \tag{2.51}$$

Normally, matrix $A(x)$ is unique just if it is composed of only one scalar. Otherwise, it can be rewritten in other parametrization of state dependent coefficients (Banks et al., 2007).

The weighting matrices $Q(x)$ and $R(x)$ are defined as positive and presented in Eq. (2.52) and Eq. (2.53).

$$Q = 10^4 \begin{bmatrix} 1 & 0 & 0 & 0 & 0 \\ 0 & 1 & 0 & 0 & 0 \\ 0 & 0 & 1 & 0 & 0 \\ 0 & 0 & 0 & 1 & 0 \\ 0 & 0 & 0 & 0 & 1 \end{bmatrix} \tag{2.52}$$

$$R = [1] \tag{2.53}$$

Equation (2.54) presents the desired states for the system. In this case, just the angular position of the beam like structure is controlled, being that the desired position is placed in 1 radian.

$$x^* = \begin{bmatrix} 0 \\ 1 \\ 0 \\ 0 \\ 0 \end{bmatrix} \tag{2.54}$$

2.6 Slewing System Analysis

In order to analyse the proposed models, numerical simulations and experimental test reproducing the simulations conditions were performed. Being that the simulations are divided in the simulation of the DC motor without load, and DC motor with load, were the load is considered the beam like structure. Next the complete and non ideal system is simulated in order to analyse the complete model behaviour.

2.6.1 DC Motor

The DC motor simulation, considers the motor without load, and with all initial conditions equal to zero. For the simulation the equations of motion of the DC motor, Eq. (2.4) and Eq. (2.5), are utilized. The simulation consist of and step of 10 V in open loop, applied to the DC motor armature. The simulation parameters for the DC motor are presented in table 2.1. These parameters was experimentally obtained by following the methodology presented in Appendix A.

Table 2.1: DC motor simulation parameters

Parameters	Values	Unit
R	4.57	Ω
L_m	$3.2\left(10^{-3}\right)$	H
K_t	0.23309	$N.m/A$
K_b	0.23309	$N.m/A$
b	$1.405\left(10^{-3}\right)$	$N.m.s/rad$
J	$2.6\left(10^{-4}\right)$	$kg.m^2$

Figure 2.5 present de electric current signal which results from the voltage step. It is possible to see that when the motor starts, a current peak appears, which can be justified through the motor shaft momentum of inertia. After 0.2 seconds, the DC motor reaches the steady state, where its current maintains the value of $0.2406A$.

In Fig. 2.6 the angular position (in radians) of the DC motor shaft for the $10V$ input is presented.

In Fig. 2.6, it is possible to see that the DC motor arrives its max speed before 0.2 seconds. This affirmation can be confirmed by analysing Fig. 2.7, which presents the speed of the DC motor for the same simulation.

It is possible to see that the DC motor arrives its steady state in about 38 rad/s, which is the maximum speed for the input step of $10V$.

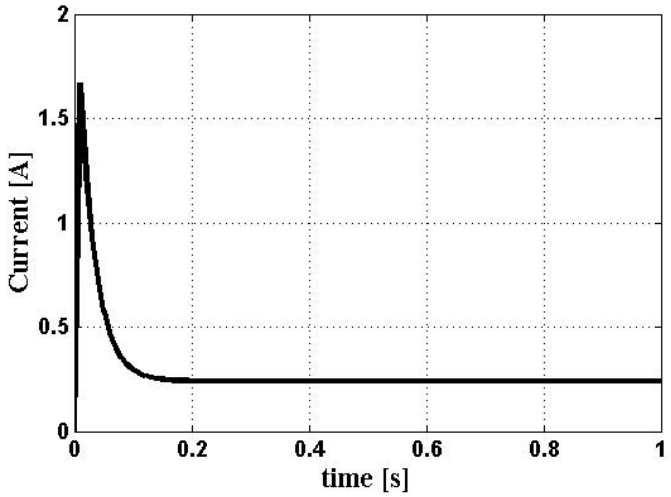

Figure 2.5: Simulation results of the electric current after an input step of 10 Volts.

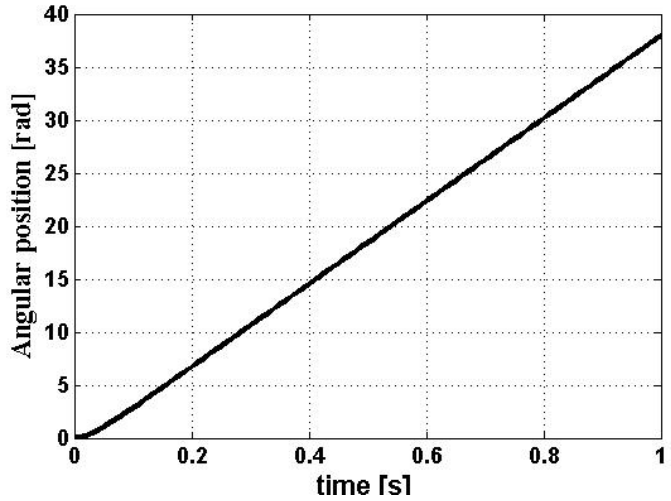

Figure 2.6: Angular displacement of the DC motor shaft for an input step of 10 Volts.

2.6.2 DC Motor Experimental Results

To validate the simulation results and the obtained parameters for the DC motor, the experimental test which reproduces the simulation was performed. A voltage step of $10V$ was applied to the DC motor without load. Figure 2.8, presents an image of the DC motor used in this work.

Figure 2.9 presents the electric current signal applied to the DC motor for the $10V$ step measured by a current sensor. As seen before, the DC motor arrives the steady state before 0.2 seconds.

By comparing the simulation results of Fig. 2.5 and Fig. 2.9, it is possible to see a

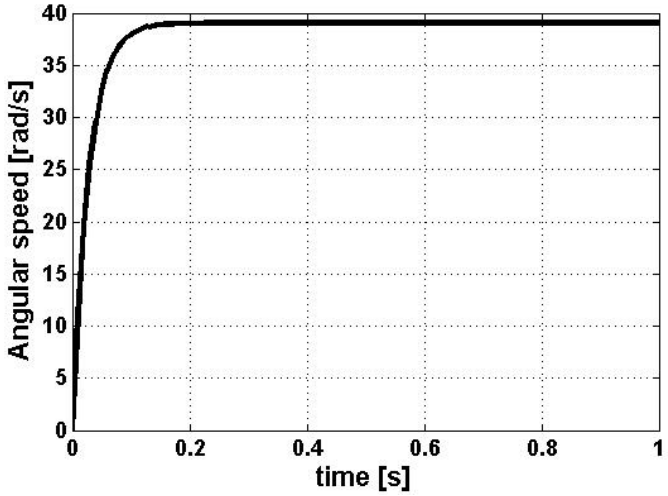

Figure 2.7: Angular speed of the DC motor for an input step of 10 Volts.

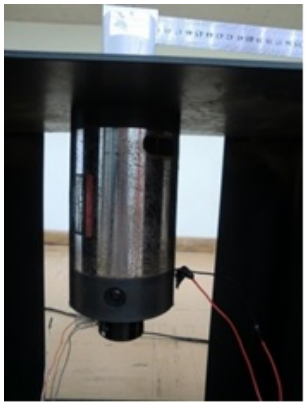

Figure 2.8: Image of the DC motor.

similarity. The steady state current for the experimental results is 0.3 Amps, which is near to the simulation results. The settling time for both cases is very close. By analyse the current peak, it is possible to see a big difference between the simulation and experimental results. This can be explained because of the difficulty to obtain the momentum of inertia and the friction coefficient of the internal parts of the DC motor.

Figure 2.10 presents the angular displacement of the DC motor shaft. By comparing they to Fig. 2.6, it is possible to see that they presents the same behaviour, with very close results.

Figure 2.11 presents the angular position of the motor shaft in degrees. This is the signal obtained from the angular position sensor.

By analysing more deeply the result in Fig. 2.10, it is possible to see that after 1 second, the DC motor shaft shifted about 38 rad. By comparing this result to the simulated speed in Fig 2.6 it is possible to assume that the simulation and experimental results have a very

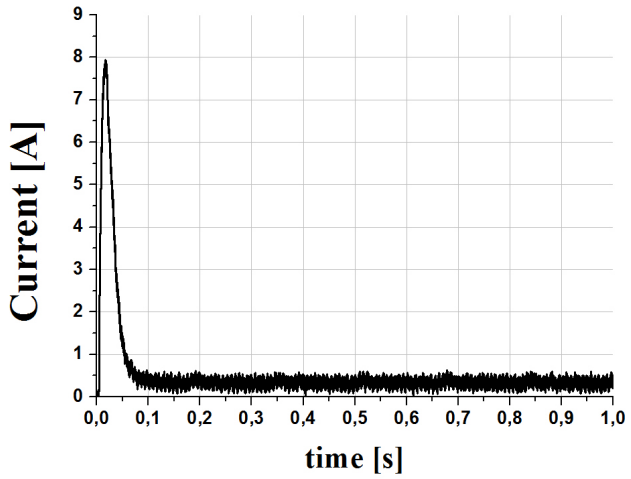

Figure 2.9: Measured electric current for a 10 Volts step applied to the DC motor armature.

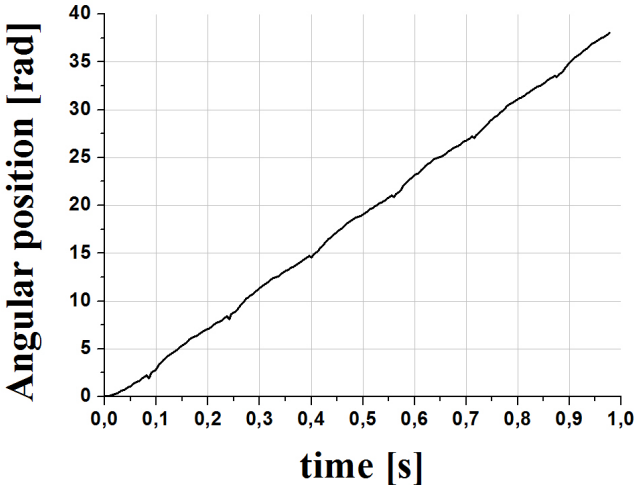

Figure 2.10: Measured angular displacement of the DC motor shaft for an input step of 10 Volts.

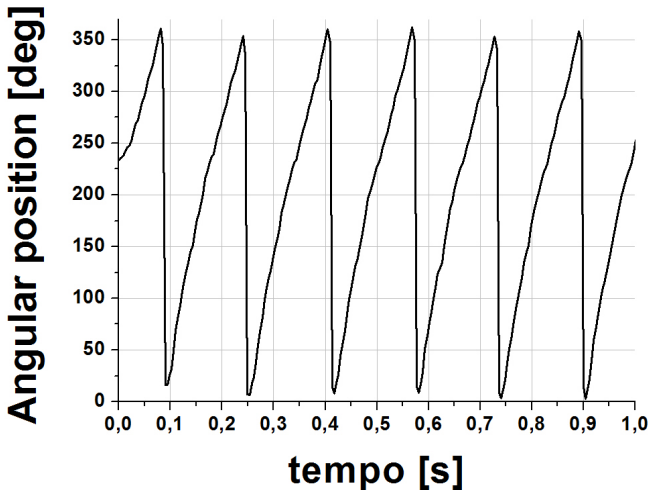

Figure 2.11: Measured angular position of the DC motor shaft for an input step of 10 Volts.

close steady state speed.

After this analysis, it is possible to assume that the chosen DC motor model and the measured parameters for the DC motor represents very closely the real DC motor dynamics.

2.6.3 DC Motor With Load Experimental Results

Considering that the flexible beam like structure is coupled to do DC motor shaft, it is important to consider the influence of the moment of inertia of this over the motor dynamics. This consideration is made by adding the moment of inertia of the flexible beam like structure to the DC motor moment of inertia. In order to validate this coupling, new simulations and experimental test was performed. Where the moment of inertia of the flexible structure is considered to be $1.1093(10^{-12})m4$. This value is obtained theoretically.

Figure 2.12 presents the simulation result for a step of 7 Volts applied to the DC motor armature. This simulation considers the influence of the momentum of inertia of the beam like structure over the DC motor. It is important to consider that over 7 Volts, the bending moment is high enough to damage the beam like structure.

It is possible to see that momentum of inertia do not have an important influence over the DC motor current. This simulation considers only the moment of inertia of the beam, the effects caused by the beam vibrations are not considered in this simulation.

Figure 2.13 presents the experimental test for the same case. It means that the beam like structure is now coupled to the DC motor shaft. It is possible to see that the steady state current measured is much more higher than the simulated current. Were this

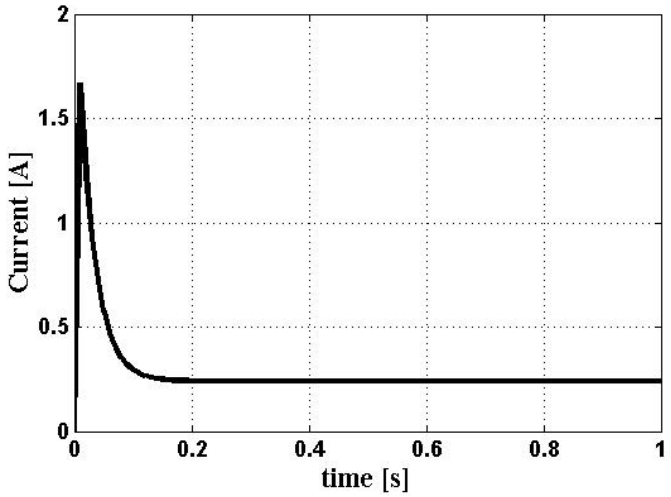

Figure 2.12: Simulation of the current applied to the DC motor armature for a step of 7 Volts.

difference is higher than 1 Amps.

The second current peak that appears in Fig. 2.13 is caused by the beam vibration coupled to the motor shaft, but do not explain the difference between the simulation and experimental results.

In the work presented by Janzen et al. (2014b), the authors suggest the inclusion of aerodynamic drag force to the model, which represents the influence of the air drag over the beam like structure. By including this term into the simulations, the result presented in Fig 2.14.

It is possible to see that the result presented in Fig. 2.14 is more closer to the result presented in Fig. 2.13.

The influence of the aerodynamic drag force is related to the angular rotation speed. How faster is this rotation higher is this influence. In other words, how faster the rotation more will the current increase.

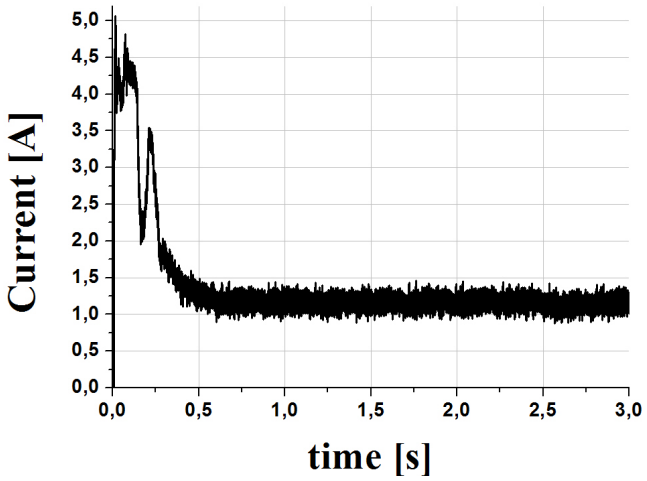

Figure 2.13: Measured electric current applied to the DC motor armature with the coupled flexible structure for a step of 7 Volts.

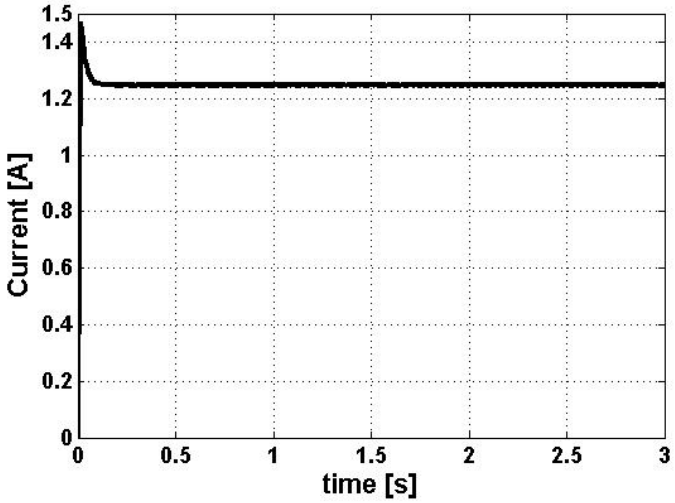

Figure 2.14: Simulation of the current applied to the DC motor shaft considering the beam moment of inertia and the aerodynamic drag force.

Chapter 3

ShapeMemory Alloys Modelling

In this chapter we will present a brief bibliographic revision, and the model proposed by (Elahinia, 2004), which is the chosen model to be applied in this thesis, is presented. Numerical simulation of the model are performed and its result will be presented and analysed. In order to analyse bather the SMA behaviour, experimental test will be performed and its results will be presented and analysed in this chapter.

3.1 Shape Memory Alloys

Many works have been presented in the last decade showing the application of actuators or intelligent structures build by materials known as intelligent materials. Materials like Piezoelectric Ceramics and Shape Memory Alloys are examples of this kind of materials. In order to control or supperss vibrations, some researches has been dedicate to apply the PZT's as actuators, because of its easy control in comparison to other materials. In his work, Yuvaraja and Senthilkumar (2013), have presented a comparison of the application of PZT and SMA as active actuators to suppers the vibrations of a cantilever beam. They results presents that the SMA actuator have a better efficiency in relation to the PZT actuator, because it needs lower control voltages and the SMA actuator is more simple to be coupled to the structure.

According to Mavroidis (2002), the SMA are between the actuators with better ratio between weight and power in the application range from $0kg$ to $10kg$.

Shape Memory Actuators, are constituted of Shape Memory Alloys connected to a mechanical device, where the actuation element is the SMA. The actuation for this kind of materials is made through the temperature change, it means, heating and cooling the material between the phase transformation temperatures.

Shape Memory Alloys applied to structures generally can be used as sensors and actuators, where they present the capacity to change the rigidity, natural frequency's between

other mechanical properties through the imposition of an electric or electromagnetic fields, temperature changes and applied stress. These composite structures normally are called as intelligent structures (Paiva, 2004).

The SMA are a metallic materials group that presents the ability to return to a previous defined form by applying an excitation signal. This phenomenon is known as shape memory effect. The shape memory effect occurs due the displacement of the crystalline structure of the material between two phases. These phases are called as martensite and austenite, where they are the low temperature and high temperature phase respectively (Piccirillo et al., 2009).

The shape memory effect is characteristic which turns possible the application of the SMA's as actuators. When this material are heated, the material crystalline structure deforms, and when cooled, the crystalline structure turns to his original form. The phase change is not a linear phenomenon presenting hysteresis characteristics (Romano and Tannuri, 2009).

The SMA non-linearity appears due the different properties of the material in the martensite and austenite phase. The crystalline structures of the material in the austenite phase, normally presents a cubic form. In the martensite phase this structures presents a tetragonal form. The change between the two phases occurs due a shear lattice distortion. This kind of material phase transformation is called as martensitic transformation (Lagoudas, 2008).

In Fig. 3.1, it is possible to see a schematic illustration that represents the crystal structure transformation. The phase transformations are limited by four characteristic temperatures, where M_s is the martensitic start temperature, M_f is the martensitic transformation finish temperature, A_s represents the austenitic start temperature and A_f is the austenitic finish temperature.

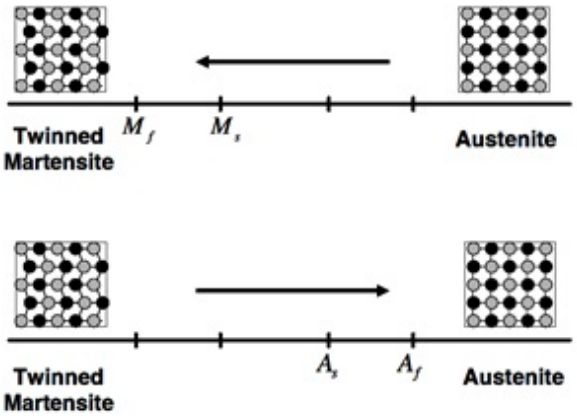

Figure 3.1: Schematic illustration representing the shape memory effect (Lagoudas, 2008).

The forward transformation, from the austenite phase to the martensite phase, starts in M_s and stops in M_f. When the temperature is under M_f, the material is completely in the twinned martensitic phase. In the reverse transformation, from martensitic phase to austenitic phase, the material is heated and the transformation starts at A_s and stops at A_f where the material is completely in the austenitic phase (Lagoudas, 2008).

When the material is in the twinned martensitic phase and a mechanical load is applied to it, it is possible to detwin the martensite, which results in a macroscopic shape change, which the deformation is retained when the load is released. This process is presented in Fig. 3.2a.

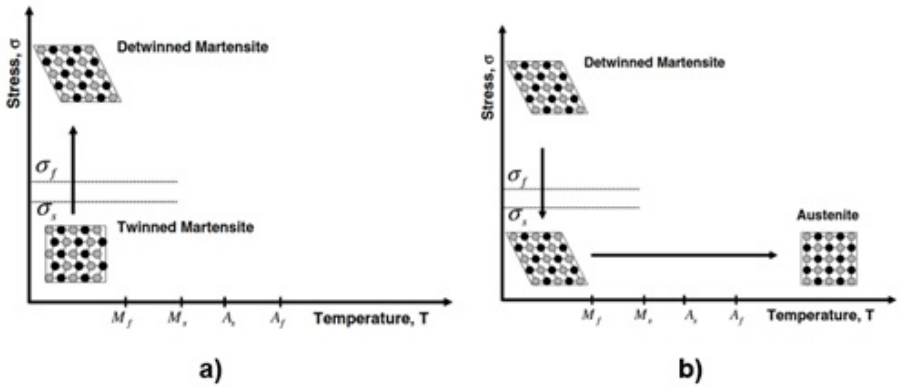

Figure 3.2: a) Schematic of the SMA detwinning process by applying stress. b) Schematic of the shape memory effect by unloading the SMA and after heating those (Lagoudas, 2008).

When the material is heated up to the austenitic start temperature as presented in Fig. 3.2b, the reverse phase transformation occurs and after cooling the material below the martensitic transformation temperature, they recovers completely his original.

The complete phase transformation process is presented in Fig. 3.3, which demonstrates a graphical representation of the stress-strain-temperature plane.

3.2 Shape Memory Alloys Actuators

Several works have shown the application of Shape Memory Alloys to suppress vibrations or to control the deflection of flexible structures. This grate interest in this kind of actuator comes up because of many advantages that the SMA actuators presents in relation to other smart materials or conventional actuators.

According to Fig. 3.4, which presents a comparison between the actuation energy density in relation to the actuation frequency, the SMA's have the higher actuation energy density's in relation to some other smart materials. That means that the SMA have a

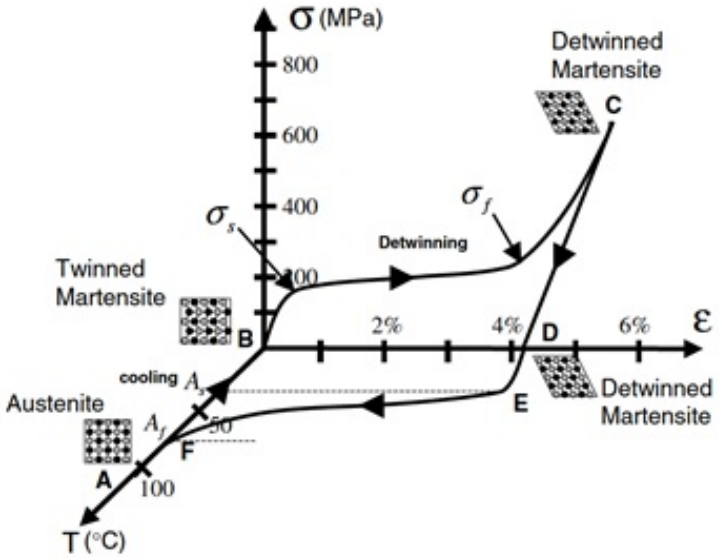

Figure 3.3: Graphical representation of the shape memory effect through a stress-strain-temperature graph (Lagoudas, 2008).

higher capacity to produce work per material volume. This characteristic shows to be very interesting when considering that a lighter and smaller actuator can apply forces equivalent to conventional actuators like DC motors, pneumatic cylinders and electric solenoids.

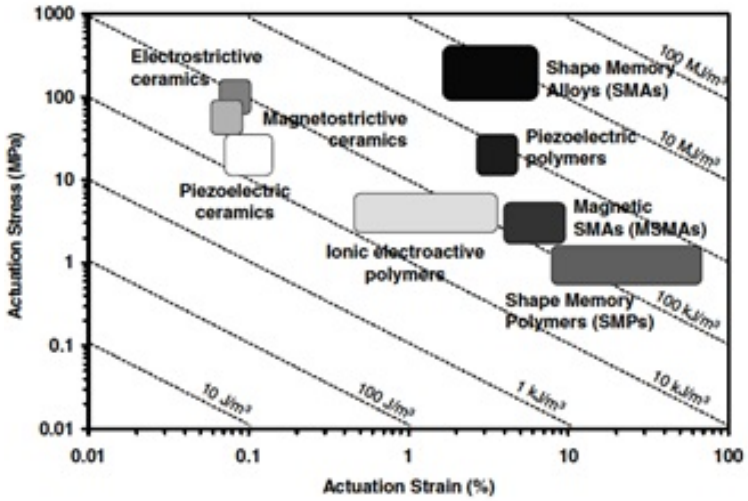

Figure 3.4: Actuation energy density of different smart materials (Lagoudas, 2008).

One disadvantage that can be seen in Fig 3.5, is the low actuation frequency's. The SMA normally actuates with temperature changes, it means, they are thermomechanical systems. It is known that temperature exchange is a slow process, which limits the response time of the SMA actuators to only a dozen hertz.

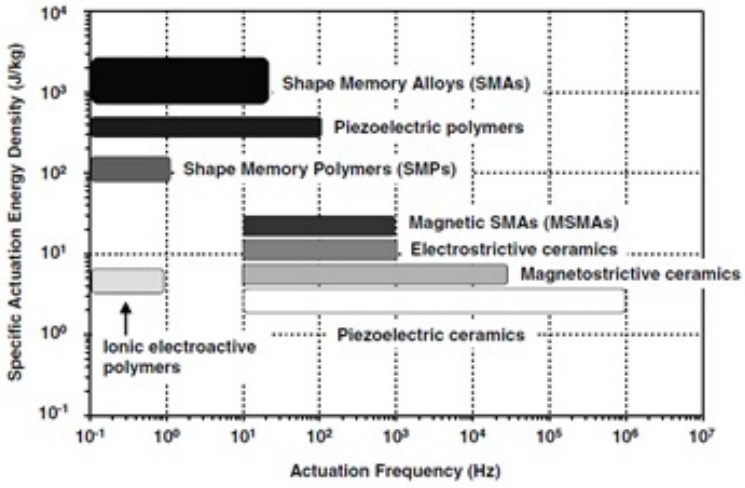

Figure 3.5: Comparison between the actuation frequencies for various smart materials (Lagoudas, 2008).

Other smart materials like PZT's have a very higher actuation frequency range, but are more difficult to be coupled and are more sensitive to mechanical impacts. The SMA's are easier to be coupled to any system because they are ductile and malleable.

In his work, Sohn et al. (2009) have presented the application of SMA wire actuators to control the position and the vibration of a flexible beam like structure. The coupled the SMA wires angled to the beam. The control of the actuators was made through the Sliding Modes control technique. Your results demonstrate that the SMA actuators are with the robust controller assure a good performance to vibration and tracking control of flexible structures.

Ge et al. (2006), propose in his work a vibration control of a flexible rotating link, by applying SMA actuators and a linear controller based on proportional and derivative (PD) gains. Janzen et al. (2015), presents in his work the control of the angular position and vibration of a slewing flexible structure by applying SMA actuators parallel and directly coupled to the flexible beam like structure. The proposed controller by them was the State Dependent Ricatti Equation (SDRE) controller. Simulation and experimental results demonstrate that this coupling form do not present good results in order to suppress the beam vibrations. They demonstrate that this coupling form presents better results in the second vibration mode.

3.2.1 Shape Memory Alloys Mathematical Models Classification

In order to better understand the SMA behavior and to study its application as actuator several models have been proposed to represent the dynamics of SMA's under different

temperature and loading conditions (Elahinia, 2004).

According to (Elahinia and Ashrafiuon, 2002), the SMA models can be classified in three categories, which are the free energy based models, the phenomenological models and the geometric models.

The phenomenological models are the most used in the study of SMA actuator applications. This is because of the simpler structure of the model and because the model parameters are possible to be measured.

3.3 Shape Memory Alloys Modelling

The SMA model chosen to be applied in this work, is a phenomenological model presented by Elahinia and Ashrafiuon (2002), which is based on the models proposed by Tanaka (1986)) and improved by Liang and Rogers (1990) and Brinson (1993). This model considers the stress generated by the SMA wire depends of the strain, temperature and transformation phase. The SMA wire constitutive model is presented in Eq. (3.1).

$$\dot{\sigma} = D\dot{\varepsilon} + \Omega\dot{\xi} + \Theta_T\dot{T} \tag{3.1}$$

Where σ is the wire stress, D is the Young modulus of the SMA material, ε is the strain, T is the material temperature, Θ_T is the thermal expansion factor, ξ is the martensitic fraction and Ω is the phase transformation contributor factor, which is described as:

$$\Omega = -D\varepsilon_L \tag{3.2}$$

where ε_L is the maximum recoverable strain.

For simulate the SMA wire constitutive equation, the martensitic fraction derivative $\dot{\xi}$ need to be calculated in each interaction of the numerical simulation algorithm. Due to the hysteresis behaviour of the SMA wire, two different equations are necessary to represent the martensitic factor. Equation (3.3), represents the reverse transformation (martensite to austenite), what means that the SMA wire will be heated.

$$\dot{\xi} = -\frac{\xi_M}{2}\sin\left[a_A\left(T - A_s\right) + b_A\sigma\right]\left[a_A\dot{T} + b_A\dot{\sigma}\right] \tag{3.3}$$

where $a_A = \frac{\pi}{A_f - A_s}$, $b_a = \frac{-a_A}{C_A}$ and A_f and A_s are the austenite finish temperature and austenite start temperature respectively. C_A is a curve fitting parameter and ξ_M is the minimum martensite fraction the wire reach during the cooling.

Equation (3.3) is calculated only when the condition presented in Eq. (3.4) is satisfied,

otherwise the derivative of the martensitic fraction derivative is null.

$$if \begin{cases} \dot{T} - \dfrac{\dot{\sigma}}{C_A} > 0 \\ and \\ \left(A_s + \dfrac{\sigma}{C_A}\right) < T < \left(A_f + \dfrac{\sigma}{C_A}\right) \end{cases} \tag{3.4}$$

Equation (3.5), represents the forward transformation (austenite to martensite), what means that the SMA wire will be cooled.

$$\dot{\xi} = -\frac{1-\xi_A}{2} \sin\left[a_M \left(T - M_f\right) + b_M \sigma\right] \left[a_M \dot{T} + b_M \dot{\sigma}\right] \tag{3.5}$$

where $a_M = \frac{\pi}{M_s - M_f}$, $b_M = \frac{-a_M}{C_M}$ and M_f and M_s are the austenite finish temperature and austenite start temperature respectively. C_M is a curve fitting parameter and ξ_A is the minimum martensite fraction the wire reach during the heating.

Equation (3.5) is calculated only when the condition presented in Eq. (3.6) is satisfied, otherwise the derivative of the martensitic fraction derivative is null.

$$if \begin{cases} \dot{T} - \dfrac{\dot{\sigma}}{C_M} > 0 \\ and \\ \left(M_f + \dfrac{\sigma}{C_M}\right) < T < \left(M_s + \dfrac{\sigma}{C_M}\right) \end{cases} \tag{3.6}$$

The Young modulus and the electric resistance of the SMA wire can be describe as presented in Eq. (3.7) and Eq. (3.8) respectively.

$$D = \xi E_M + (1 - \xi) E_A \tag{3.7}$$

$$R_{SMA} = \xi R_M + (1 - \xi) R_A \tag{3.8}$$

The heat transfer model equation, presented in Eq. (3.9), is composed of an electrical heating (Joule effect) component and a natural convection component.

$$\dot{T} = \frac{\frac{{V_{SMA}}^2}{R} - hA_{SMA}\left(T - T_{in}\right)}{mc_p} \tag{3.9}$$

3.4 SMA Numerical Simulation

To analyse the behaviour of the model presented in section 3.2, numerical simulations of a system composed of a mass suspended by an SMA wire were performed. This system

is presented in Fig. 3.12 and its dynamics equations can be written as:

$$m\ddot{x} + mg = F_{SMA} \tag{3.10}$$

$$\dot{\varepsilon} = \frac{-\dot{x}}{l_{SMA}} \tag{3.11}$$

where m is the mass, g the gravity an F_{SMA} is the force generated by SMA wire due the phase transformation. Table 3.1 presents the values for the simulation parameters of the system proposed in Fig. 3.12.

Table 3.1: Shape Memory Alloy simulation parameters

Parameters	Values	Unit
E_M	$75\left(10^9\right)$	N/m^2
E_A	$28\left(10^9\right)$	N/m^2
M_s	52	°C
M_f	42	°C
A_s	68	°C
A_f	78	°C
A_SMA	$5\left(10^{-9}\right)$	m^2
h	54	$W/\left(m^{2\circ}C\right)$
R_M	4	Ω
R_A	3.6	Ω
l_SMA	0.15	m
g	9.8	m/s^2
C_M	$10.3\left(10^6\right)$	$MPa/$°C
C_A	$10.3\left(10^6\right)$	$MPa/$°C
Θ	-0.055	$MPa/$°C
ε_0	0.02678	
T_in	20	°C
σ_in	$75\left(10^6\right)$	Pa
ξ_A	0	
ξ_M	1	

Figure 3.6 presents the result for the simulated temperature, which is given by Eq. (3.9), which represents the heat transfer model.

The temperature change happens due a current step of 0.9 Amps applied to the SMA wire during 50 seconds as presented in Fig. 3.7. The temperature initiates at 20°C, which is the chosen ambient temperature. The cooling of the SMA wire occurs due natural convection.

Figure 3.7 presents the current step applied to the SMA wire. It is possible to see that when the temperature arrives the austenite start temperature, by arriving the conditions presented in (3.4), the current starts to increase. This occurs due the reverse transformation,

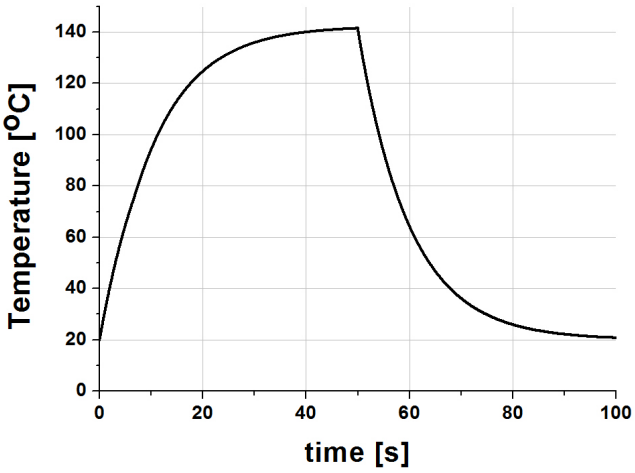

Figure 3.6: Simulated temperature signal for a current step of 0.9 Amps, with a load of 0.2 kg.

which changes the crystalline structure of the SMA, changing also the material resistivity.

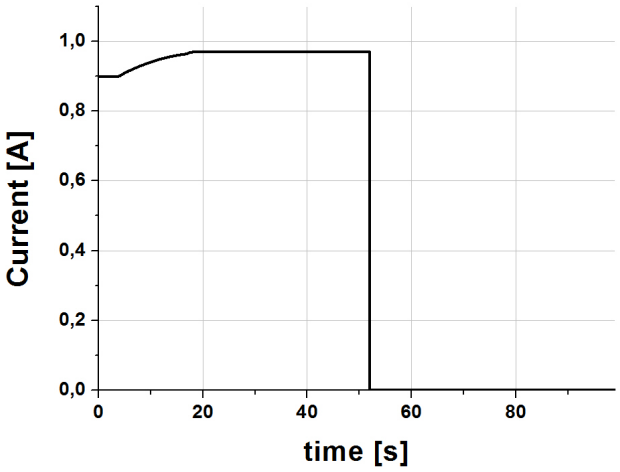

Figure 3.7: Current step applied to the SMA wire.

Figure 3.8, presents the martensitic fraction volume. It is possible to observe that after 18 seconds, the SMA wire is totally transformed in to the austenite phase. And after 60 seconds, the forward transformation starts, but the wire does not transform totally back to martensite phase. It is possible to see that a residual strain remains after the cooling time.

In order to analyse the behaviour of the SMA wire in relation to the applied electric current, a simulation was performed, in which the current is increased to 1.3 Amps and than decreased again to 0 Amps, as presented in Fig. 3.9.

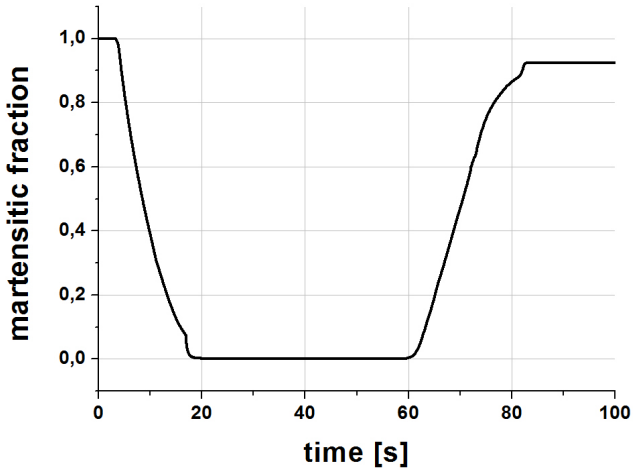

Figure 3.8: Martensitic fraction for a current step of 0.9 Amps, and a load of 0.2 kg.

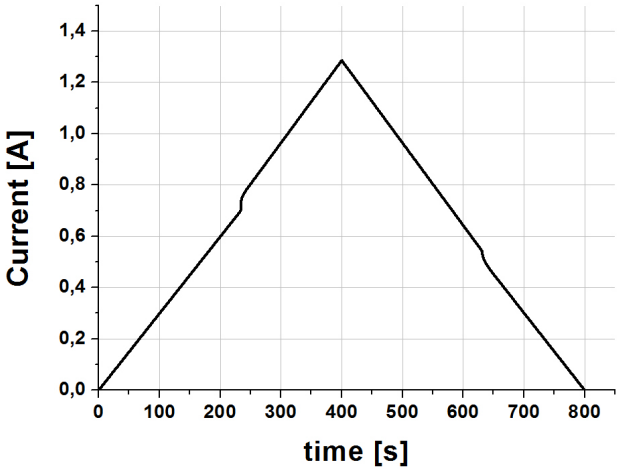

Figure 3.9: Current ramp applied to the SMA wire.

The simulation result for the applied current signal presented in Fig. 3.9, is shown in Fig. 3.10. It is possible to see the hysteresis characteristic due to two different phase transformations equations.

By analyse the forward transformation, it means from austenite to martensite, it possible to see the residual strain which remains after the transformation stop.

In order to analyse the influence of the load mass over the SMA wire phase transformation, a second simulation was performed where the mass was increased from 0.2 kg to 0.5 kg. The same current ramp signal which is presented in Fig. 3.9 was applied to the SMA. Figure 3.11 presents the comparison between the two simulation results.

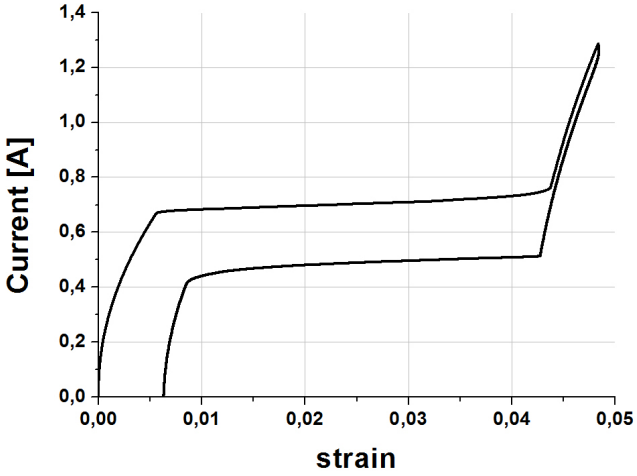

Figure 3.10: Simulation result presenting a strain per current graph for an applied current ramp.

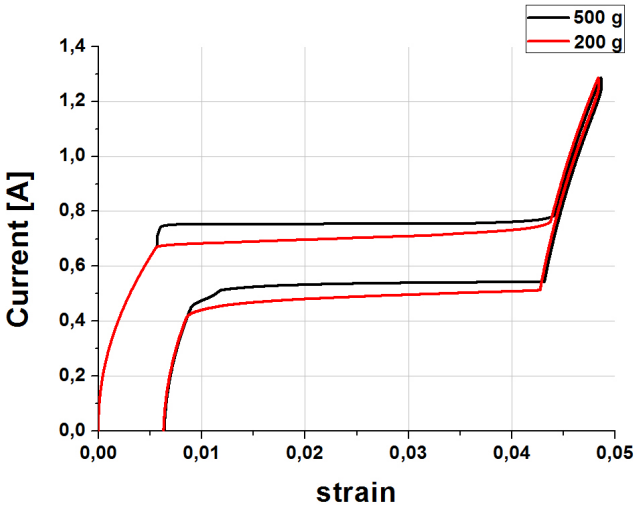

Figure 3.11: Comparison of the behaviour of the SMA wire for two different loads and the same applied current ramp.

It is possible to see in Fig. 3.11 that the increase of the load mass have a direct effect over the phase transformation current. It is seen that with the mass increase, the current needed to transform the SMA wire from the martensite phase to the austenite phase is higher than for a lower mass. In addition, for the transformation from the austenite to martensite phase the transformation starts before than for a lower mass.

3.5 SMA Characterisation Experimental Set-up

With the objective to validate the SMA chosen model an experimental system was built to perform the validation test, and to analyze the SMA behavior.

The experiment consist of a mass suspended through a SMA wire. This wire can be actuated through an electric current provided by a tunable power source. This electric current through the Joule effect heats up the SMA wire. The temperature can be controlled indirectly by controlling the electric current applied to the wire.

For this work the SMA actuator is a SMA wire commercially called as Flexinol and produced by Dynalloy INC.. This is an Alloy composed of nickel and titanium (NiTi). The Flexinol wire chosen for this work is a 0.375 mm diameter wire which have the capacity to generate a force up to 12 N.

An inductive sensor located under the suspended mass, measures the displacement of the mass when the phase transformation of the SMA occurs. Figure 3.12 presents a schematic illustration of the experimental system.

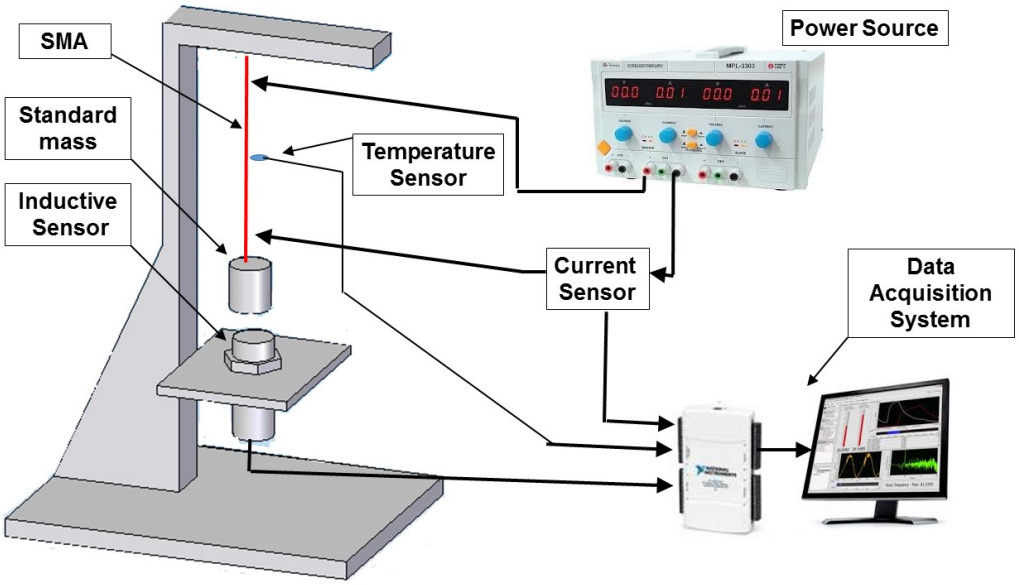

Figure 3.12: Schematic illustration of the experimental system developed to validate the SMA actuator model.

The current applied to the SMA wire is measured by a current sensor and can be controlled by the power source.

In order to analyse the relation between current and temperature, a temperature sensor was coupled beside the SMA wire. By considering that the SMA wire have just 0.375 mm of diameter its thermal mass is very low which makes the process of measure the temperature a problem. Normal temperature sensors have like Thermocouples and Thermoresistive sensors have a low response time, which is an important variable to be

measured in this thesis. To solve this problem a temperature sensor based on fiber optic technology was implemented. The Fiber Bragg Gratings (FBG) sensors are a class of sensor based on the refraction of the light in the fiber optic core. This kind of sensors can be applied to measure temperatures with a very high response time, and very low temperature variations.

Figure 3.13 presents an image of the experimental system.

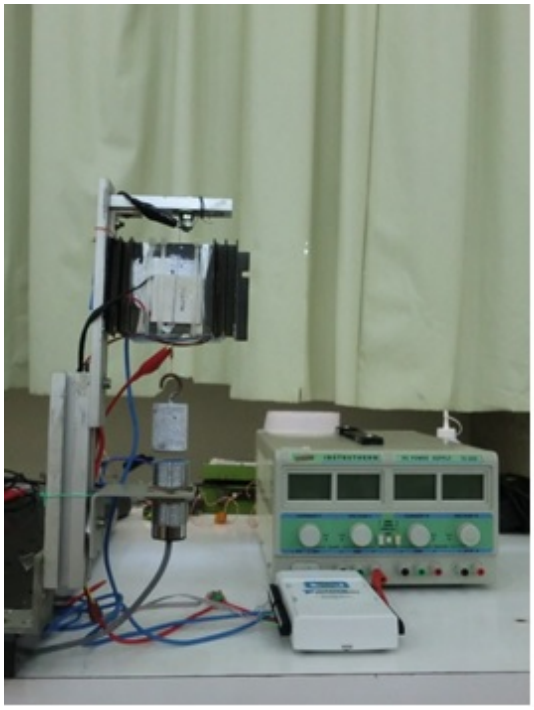

Figure 3.13: Image of the built system for the SMA actuator validation.

All the sensors where coupled to a data acquisition system Usb DAq 6212 produced by National Instruments. The data are collected, displayed, treated and saved through a software written by the LabView programming language.

3.6 Experimental Results

To analyse the SMA wire behaviour, some experimental test were performed. This test consist in apply different currents, in step and ramp, and apply different loads to the SMA wire.

In Fig. 3.14 the temperature behaviour of the SMA wire for a current step of 0.75 Amps is presented.

It is possible to see in Fig. 3.14 that the temperature behaviour changes between the phase transformation regions. The transformation from the martensite phase to the austenite phase occurs between 68°C and 78°C, being that after 17 seconds the SMA wire

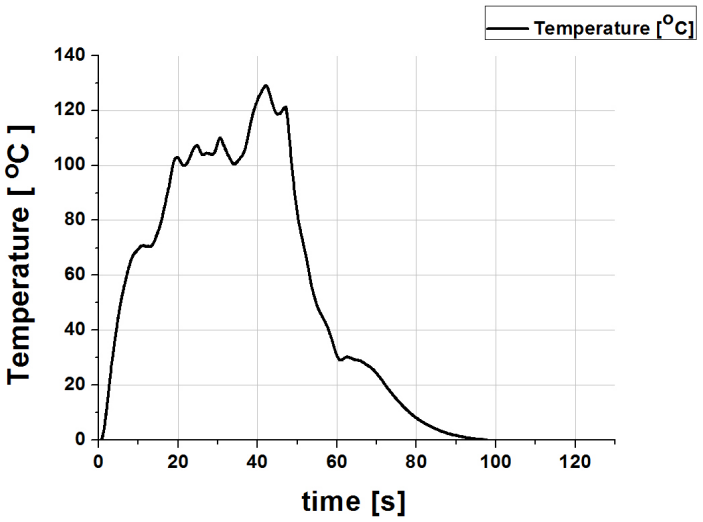

Figure 3.14: Temperature of the SMA wire for a current step of 0.75 Amps.

is completely in the austenite phase. The phase transformation from the austenite phase to the martensite phase occurs 52°C and 32°C, which is different from the expected. The expected martensitic finish temperature was 42°C. The temperature behaviour change at the phase transformation regions can be explained through the electric resistivity variation of the material due the phase transformation. This effect is better seen in Fig. 3.15.

Figure 3.15 presents the current step of 0.75 Amps, which is applied to the SMA wire whose temperature is presented in Fig. 3.14. It is possible to see a current increase during the phase transformation. This current increase can be explained through the resistivity change of the wire. For this experiment the voltage applied to the wire was kept constant, so according to the Ohm's Law, $V = RI$ to occur this change, the electric resistance need to decrease. Figure 3.16, presents the comparison between the current step and the measured temperature. It is possible to confirm that the relation between the current change and the temperature behaviour change during the phase transformation.

To analyse the effect of the current magnitude over the SMA behaviour, a second test was performed, which consist of applying different current value steps to the SMA wire. Figure 3.17 demonstrates the results for three different current steps which are respectively 0.6 Amps, 0.65 Amps and 0.8 Amps.

It is possible to see that the higher the current step value so faster is the SMA response time and higher is the strain. It is important to consider that for the SMA wire used in this work the maximum current suggested to be applied by the manufacturer is 2.5 Amps for a wire of 1 m. Very high currents applied for a long time can over heat the SMA and make it loses the memory effect.

It is possible to see also that the cooling time depends of the arrived temperature, it

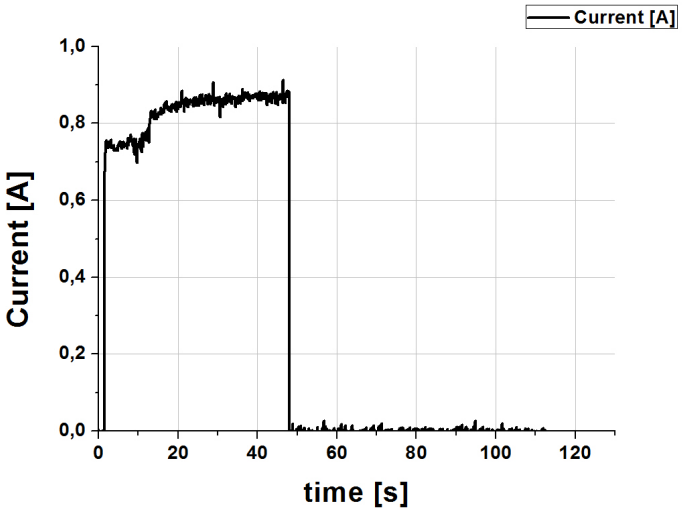

Figure 3.15: Electric current step applied to the SMA wire.

means, how higher reached temperature so longer is the cooling time and higher is the actuator response time. Figure 3.17 demonstrates the limitation for the application of the SMA wire actuators in relation to its response time.

To analyse the relation between electric current and strain, a current ramp was applied to the SMA wire. This test consists of increasing slowly the voltage applied to the wire until they is completely transformed. After the complete transformation, the applied voltage is decreased slowly until it reaches the zero. Figure 3.18 present the measured current for this test.

The relation between the electric current Fig. 3.18 and the strain is presented in Fig. 3.19. It is possible to see a hysteresis behaviour, which comes from the different physical properties of the martensite and austenite phases. By the reverse transformation, the strain change under 0.6 Amps and over 1 Amps is due the thermal expansion of the material. Between these current values, the strain change is due the phase transformation. The same analysis can be made for the forward transformation, where the phase transformation occurs between 0.8 Amps and 0.3 Amps.

In order to analyse the influence of the load mass over the phase transformation current, a third test was performed by increasing the load to 0.5 kg. The result are presented in Fig. 3.20.

It is possible to see that the load influences the phase transformation, meanly the forward transformation.

Comparing the results obtained through numerical simulation Sec. 3.4 whit the experimental results presented in Sec. 3.6, for the SMA wire, it is possible to affirm that the SMA mathematical model presented in Sec. 3.3 presents a similar behaviour to the

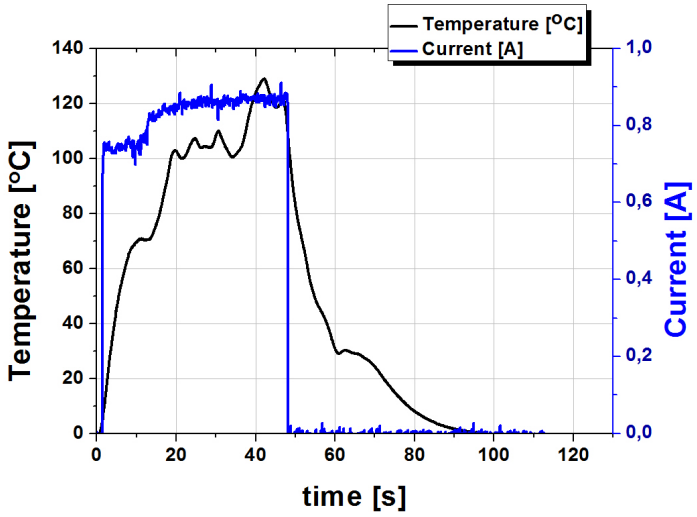

Figure 3.16: Graph comparing the current step and temperature signal due this step applied to a SMA wire.

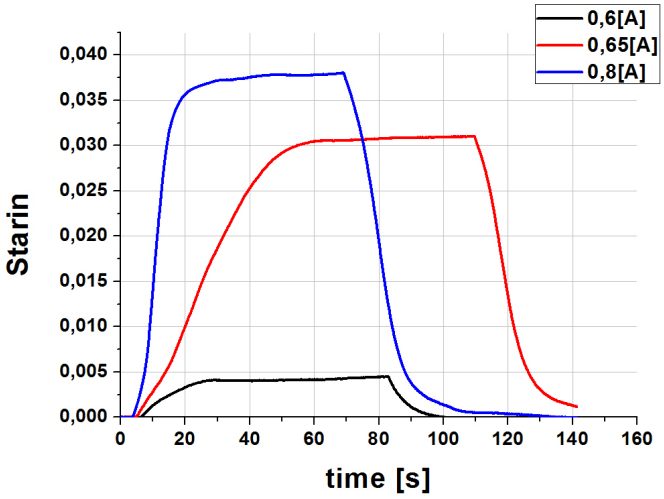

Figure 3.17: Graph comparing the SMA behaviour for different current steps values.

experimental results.

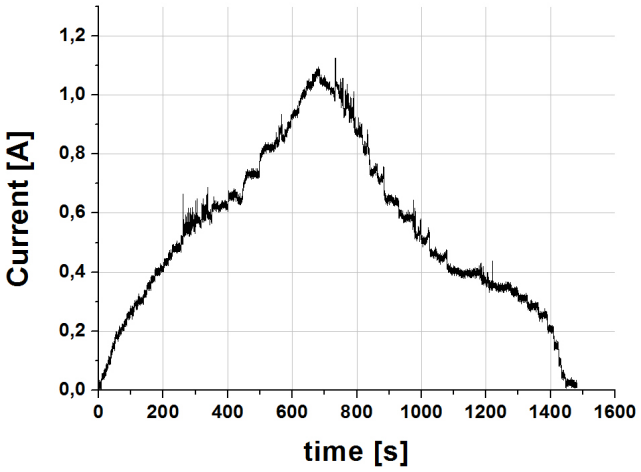

Figure 3.18: Measured current ramp applied to SMA wire.

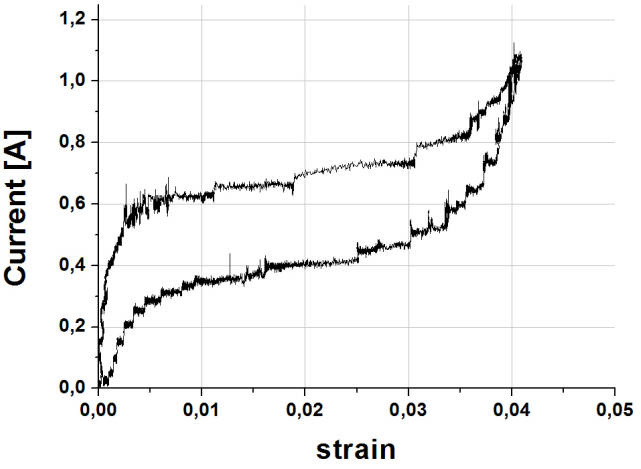

Figure 3.19: Hysteresis behaviour of the SMA wire.

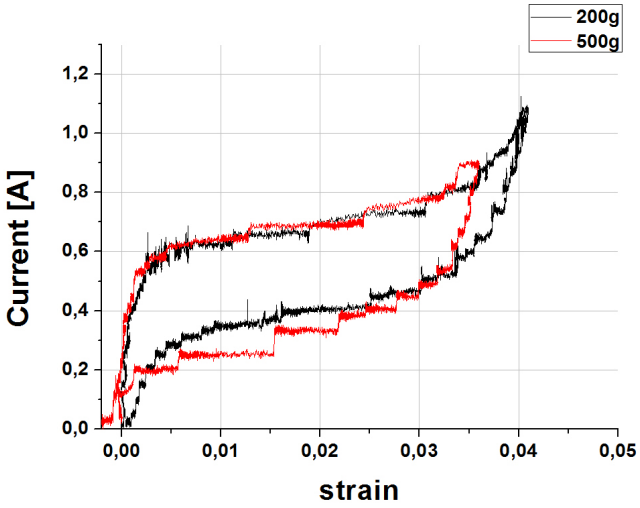

Figure 3.20: Comparison between the hysteresis behaviours for different mass loads.

Chapter 4

Parallel Shape Memory Alloy Actuator

This chapter will propose a model which couples the SMA actuator to the flexible structure in order to reduce the structure vibrations. This vibrations occurs due the slewing of its structure. We will propose a model which permits to analyse the influence of the SMA actuator over the flexible structure in order to turn possible the project of controller for the vibration control. We will present a simple proportional controller for the vibration control with the intend to demonstrate the actuation effects of the SMA over the flexible structure. Numerical simulation will be preformed and its results analysed and commented in this chapter.

4.1 Parallel Shape Memory Alloy actuator coupling model

Many works have presented the application of SMA actuators to suppers vibrations in flexible structures. In this work, the coupling between the flexible beam like structure and the SMA actuator is considered as proposed in Janzen et al. (2015). Figure 4.1 presents schematic of this coupling method.

The coupling between structure and actuator is considered to be like as a bimetallic structure, where the two components are fixed in parallel to each other. It is considered that the length and high of the SMA actuator and flexible structure are the same. The thickness of the SMA actuator is considered very thin in relation to the flexible structure thickness.

The interaction between the structure and the SMA actuator is considered to be limited to the strain energy coupling. This affirmation is valid because of the before mentioned characteristic that the thickness of the SMA actuator is very thin in relation to the beam

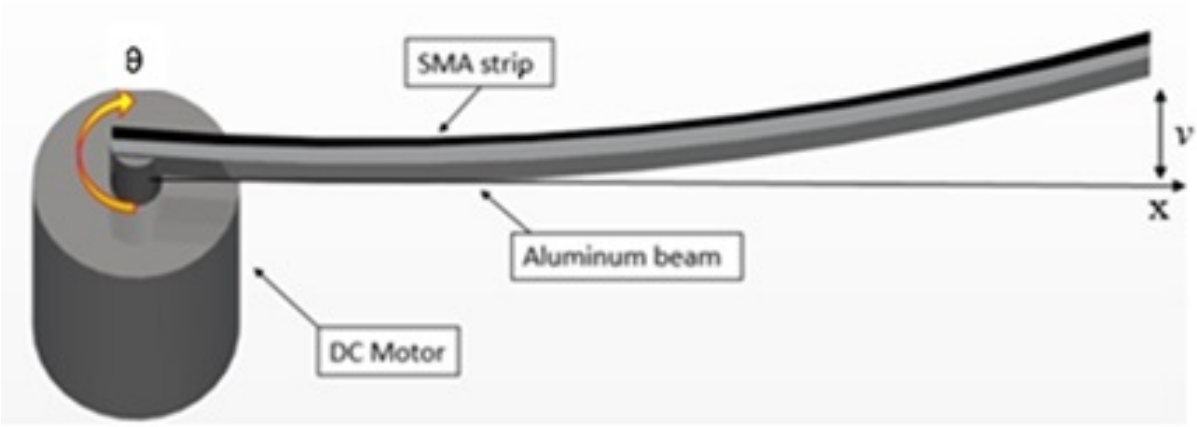

Figure 4.1: Schematic of the proposed slewing model for a SMA actuator coupled parallel to the beam like structure (Janzen et al., 2015).

structure. This affirmation turns possible to neglect the actuator moment of inertia. This work don't considers the effects of slip between the two structures.

By considering the coupling between both, structure and SMA actuator, and its models presented in chapter 2 and 3 respectively, we can say that when the SMA is heated or cooled the generate stress is coupled to the beam like structure. The opposite consideration is valid, that is, the stress due to the flexible beam displacement is coupled to the SMA actuator.

The stress for a cantilever beam can be described as the ratio between the bending moment and the moment of inertia of the beam. The bending moment can be described can be described as showed in Eq.(4.1). This work considers only the first vibration mode (Garcia and Inman, 1990a).

$$M_f = EI\phi_1{}''(0)\,\dot{q}_1 \tag{4.1}$$

The area moment of inertia for the beam can be written as in Eq. (4.2).

$$I = \frac{bh^3}{12} \tag{4.2}$$

where b is the beam thickness and h is the beam high.

The strain for a beam structure can be described as:

$$\varepsilon_v = \frac{M_f z}{IE} \tag{4.3}$$

where z is the distance from the center of the beam to the point where the strain is measured. In this work, z is considered to be the half of the thickness.

The relation between strain and stress for a beam is presented in Eq. (4.4).

$$\sigma_v = \varepsilon_v E \tag{4.4}$$

As mentioned in start of sec. 4.1, the thickness of the SMA actuator is considered very thin compared to the beam, so it is possible to affirm that the strain of the SMA actuator can be written as:

$$\varepsilon = \frac{(M_f z)}{I E_t} \tag{4.5}$$

Where E_t represents the effective Young modulus of the set SMA actuator and beam like structure, which can be described as presented in Eq. (4.6) (Ramos et al., 2007).

$$E_t = \frac{E^2\left(\frac{t_f}{t}\right)^4 + D^2\left(\frac{t_s}{t}\right)^4 + 2ED\left(\frac{t_f}{t}\right)\left(\frac{t_s}{t}\right)\left[2\left(\frac{t_f}{t}\right)^2 + 2\left(\frac{t_s}{t}\right)^2 + 3\left(\frac{t_f}{t}\right)\left(\frac{t_s}{t}\right)\right]}{E\left(\frac{t_f}{t}\right) + D\left(\frac{t_s}{t}\right)} \tag{4.6}$$

In Eq. (4.6), t_f,t_s and t, represents respectively the beam thickness, the SMA thickness and the total thickness of the set.

The bending moment of the SMA actuator can be described as presented in Eq. (4.7).

$$M_{SMA} = \sigma I \tag{4.7}$$

It is possible to consider that the total bending moment of the set, can be described as the sum of the two bending moments as presented in Eq. (4.8).

$$M_t = M_f + M_{SMA} \tag{4.8}$$

By analysing Eq. (4.8), we can assume that when the SMA actuator is activated and the bending moment of the beam is negative, the total bending moment of the structure reduces. It means that when the displacement of the beam like structure is to the opposite side of the actuator and the SMA actuator is heated and the reverse phase transformation occurs, the actuator will pull the beam to the opposite side.

It is important to consider that because of the Young modulus change of the SMA during the phase transformation, the natural frequency of the set will change as presented in Eq. (4.9).

$$\omega_i = (a_i L)^2 \sqrt{\frac{EI}{\rho L^4}} \tag{4.9}$$

The equations of motion for the system composed of the DC motor, flexible beam like structure and SMA actuator are described in Eq. (4.10).

$$\begin{aligned}
\dot{x}_1 &= -\frac{R}{L_m}x_1 + \frac{u}{L_m} - \frac{K_b}{L_m}x_3 \\
\dot{x}_2 &= x_3 \\
\dot{x}_3 &= -\frac{b}{J}x_3 + \frac{K_t}{J}x_1 - \frac{M_t}{J} \\
\dot{x}_4 &= x_5 \\
\dot{x}_5 &= -\mu x_5 - {\omega_l}^2 x_4 + \alpha_l \dot{x}_3 - {x_3}^2 x_4 \\
\dot{T} &= \frac{\frac{{V_{SMA}}^2}{R} - hA_{SMA}\left(T - T_{in}\right)}{mc_p} \\
\dot{\sigma} &= D\dot{\varepsilon} + \Omega\dot{\xi} + \Theta_T\dot{T} \\
\dot{\varepsilon} &= \frac{\left(EI{\phi_1}''q_1 z\right)}{IE_t}
\end{aligned} \tag{4.10}$$

where q_1 is equal to x_5.

4.2 Numerical Simulation Results

The numerical simulations where performed in LabView, where the integration method used is a 4th order Runge Kutta integrator. The simulation parameters for the system are presented in Tab. 2.1 and Tab. 3.1.

The initial conditions for the simulation considers that the system is in at rest, it means that the motor is stopped, the beam like structure is not deflected and the SMA actuator is totally in the martensite phase at the ambient temperature.

4.2.1 Angular Positioning Control

In order to analyse the dynamic behaviour of the proposed system and analyse the model developed numerical simulations of the model were performed. Figures 4.2 to 4.5 show the results for the system simulations only control of the angular position of the motor shaft for the SDRE controller proposed in section 2.5.

Figure 4.2 presents the electric current applied to the DC motor armature for a displacement of 1 radian of the motor shaft.

In Fig. 4.3, the displacement of the beam like structure due the position control. This work considers only the first vibration mode.

It is possible to see by analyse Fig. 4.2 various several current peaks. The first peak happens because the moment of inertia and viscous friction of the DC motor shaft and the

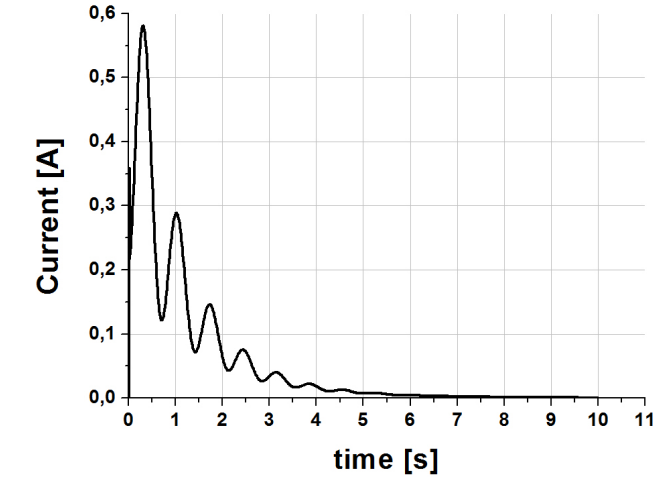

Figure 4.2: Simulated electric current applied to the motor shaft for the position control.

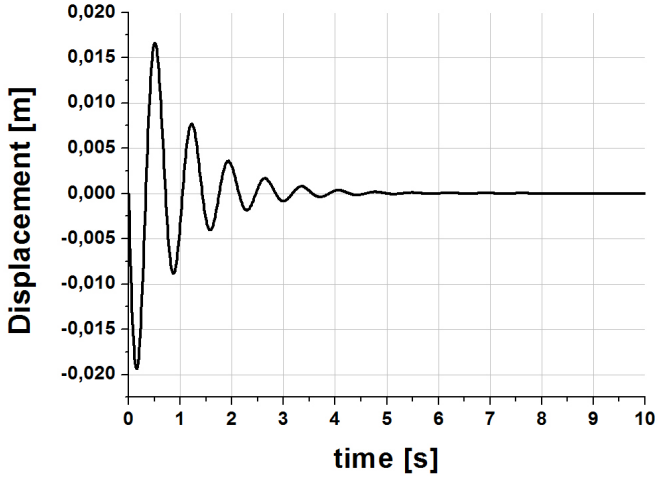

Figure 4.3: Simulation of the flexible beam displacement for the 1 radian displacement of the motor shaft.

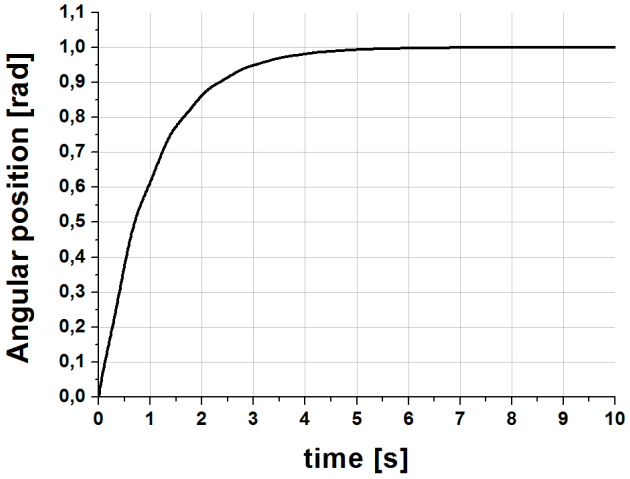

Figure 4.4: Simulation of the angular position of the DC motor shaft.

moment of inertia of the beam like structure. The other peaks can be explained through the bending moment of the beam like structure which is coupled to the motor shaft. This can be assumed by analysing Fig. 4.3, which presents the beam displacement. It is possible to see that the current peaks of Fig. 4.2 are in opposite phase to the peaks of Fig. 4.3.

Figure 4.4, presents the angular position of the motor shaft, which is controlled through the SDRE controller to go to the desired position (1 radian). It is possible to see that the system arrives the desired position at 5.8 seconds without overshoot.

In Fig. 4.5, the temperature of the SMA actuator is presented.

It is possible to see that without actuation the temperature remains the same as the ambient temperature.

4.2.2 Angular Positioning and Vibration Control

In order to analyse the effect of the SMA over the slewing structure, this work propose a proportional controller to suppress the vibration of the flexible beam trough applying a electric current to the SMA actuator.

The proposed control is presented in Eq. 4.11.

$$V_{SMA} = K_p q_1 \tag{4.11}$$

where V_{sma} is the voltage applied to control the SMA actuator temperature as presented in Eq. (4.11), K_p is the proportional gain and q_1 is the beam displacement.

It is possible to see in Fig. 4.6, which presents the current applied to the DC motor, that the current applied to control the angular position is practically the same as the

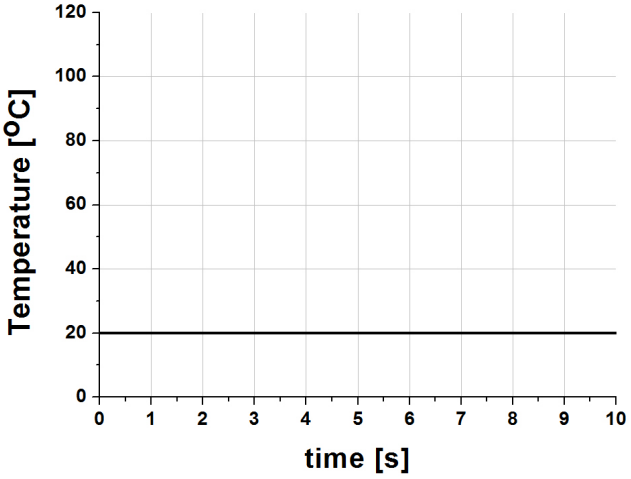

Figure 4.5: Simulated SMA temperature.

applied for the system without SMA control.

Figure 4.7 presents the angular position displacement of the system. It is possible to see that the SMA actuator don't influences significantly the angular displacement when comparing Fig. 4.7 with Fig.4.4.

In Fig. 4.8, the displacement of the beam like structure due the position control considering a SMA actuator in vibration control. This work considers only the first vibration mode.

In Fig. 4.9, is presented the displacement of the beam like structure due the position control considering two cases, with a SMA actuator in vibration control and without SMA actuator.

Can be seen in Fig. 4.9, with SMA actuator occurred a reduction of the amplitude displacement and a phase alteration in vibration, behaviour also observed in Raghavan et al. (2010).

In Fig. 4.10, the variation of the temperature of the SMA actuator is presented.

It can be seen in Fig. 4.10, that in this case the variation of the temperature, which is necessary to change the SMA stress, is necessary for reduction of the vibration amplitude of the beam.

In Fig. 4.11, the variation of the martensitic fraction by considering the temperature change applied during the control Fig. 4.10 is presented.

Analysing the results presented in Fig. 4.11, it can be observed that a phase change occurs, firstly from (martensite to austenite) and posteriorly from (austenite to martesite), adequate behaviour for the where the material temperature varies over the austenite phase start temperature.

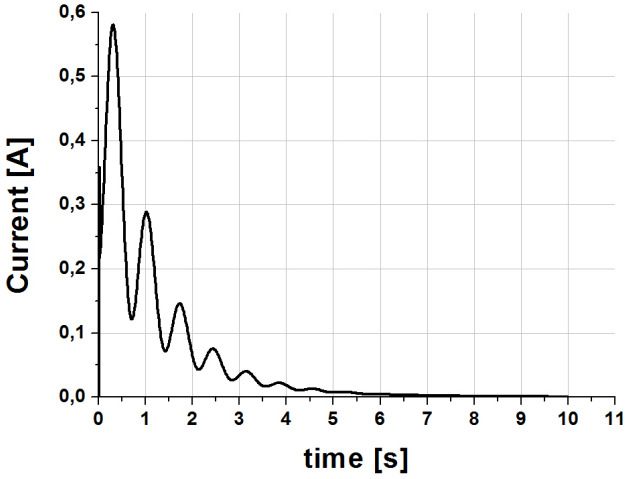

Figure 4.6: Simulated electric current applied to the motor shaft for the position control.

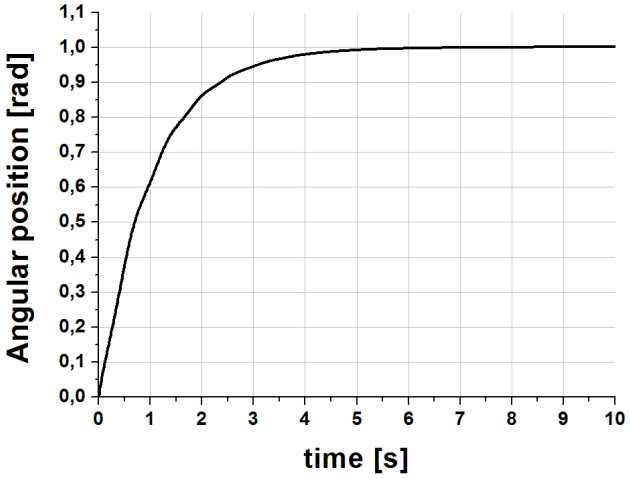

Figure 4.7: Simulation of the angular position of the DC motor shaft.

Figure 4.12, presents the voltage variation applied to change the SMA temperature by considering the case where the vibration is controlled.

It is possible to see Fig. 4.12, that when the beam displacement in Fig. 4.8 is positive the voltage applied to the SMA actuator is proportional to the displacement of the beam. When the beam displacement is negative, the voltage applied to the SMA actuator is null.

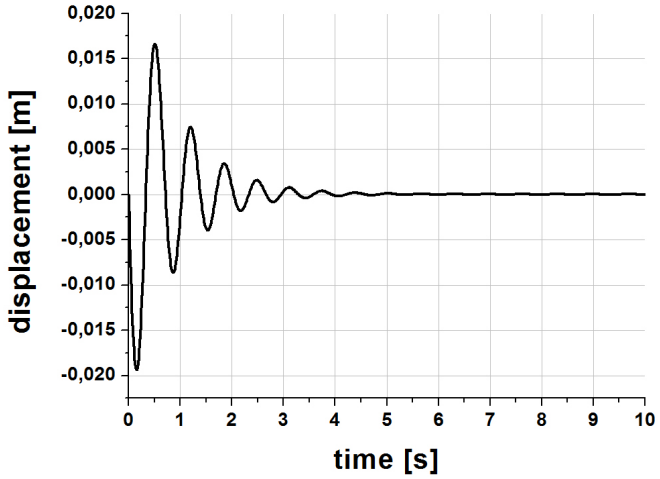

Figure 4.8: Simulation of the flexible beam displacement for the 1 radian displacement of the motor shaft.

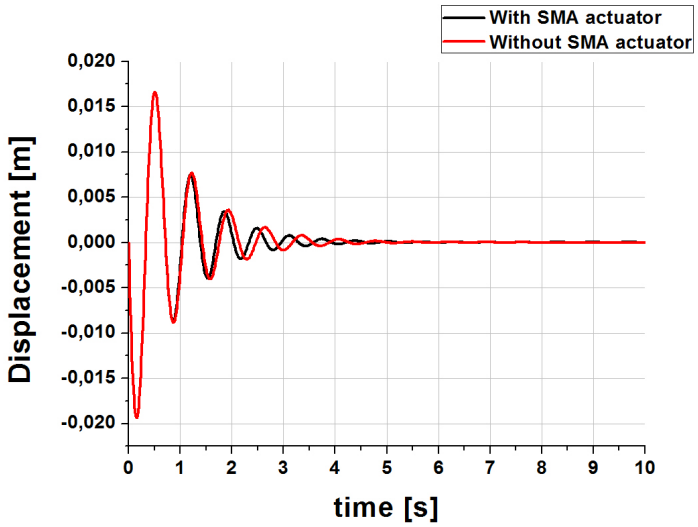

Figure 4.9: Comparison between the beam displacement for the system with and without the SMA actuation.

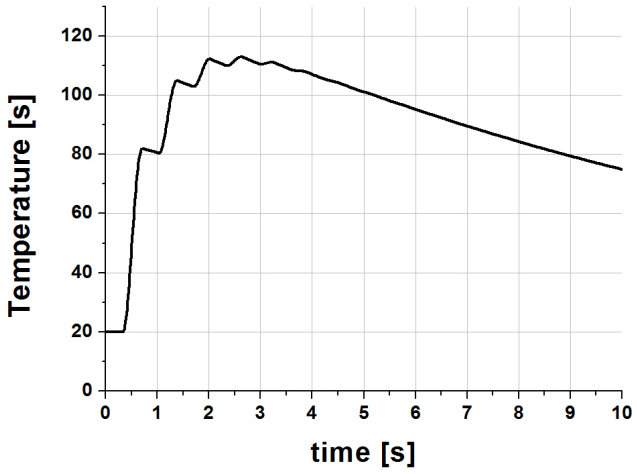

2.jpg

Figure 4.10: Simulated temperature of the actuated SMA actuator.

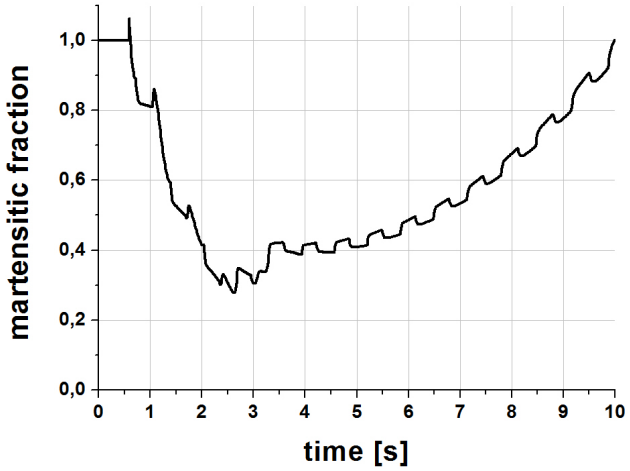

Figure 4.11: Simulated Martensitic fraction of SMA actuator.

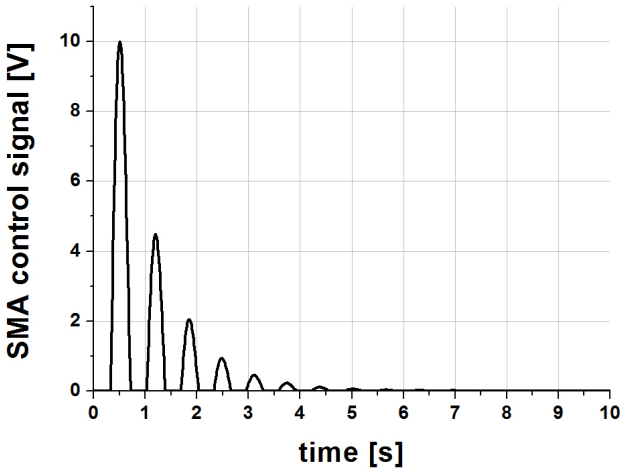

Figure 4.12: Control signal applied to the SMA actuator by the proportional controller.

Chapter 5

Experimental System

In this chapter, we will investigate experimentally the SMA actuator applied to control the vibration of a flexible structure in slewing motion. The results presented in chapter 4 will be reproduced experimentally and analysed. The experimental setup development will be explained with more details.

5.1 Experimental Set-up

To validate the model presented in chapter 4, an experimental system is mounted. This system is composed of the permanent magnet DC motor, and an aluminium beam directly coupled to the DC motor shaft, and a SMA wire, which is coupled to the aluminium beam.

The dimensions of the beam are $0.5m$ length, $0.025m$ high and $0.001m$ thick. The aluminium beam with these dimensions presents the characteristic to be flexible, which is the desired characteristic for this thesis.

The SMA wire is a NiTi (Nickel Titanium) with is called commercially as Flexinol and produced by Dynalloy, Inc.. The SMA wire is coupled in the middle of one side of the aluminium beam, where it is fixed only to the beam-ends. This wire has the following characteristics presented in table 5.1.

Table 5.1: Shape Memory Alloy wire parameters

Parameters	Values	Unit
$Diameter$	0.000375	m
$Length$	0.5	m
$LinearResistence$	8	Ω/m
$Density$	6450	Kg/m^3
$Maximumcontractiontime$	1	sec
$Relaxationtime$	13	sec
$Maximumdeformationratio$	8	$percent$
$Maximumpullforce$	1.28	N

The other parameters, like phase transformation temperature are presented in Tab. 3.1. Figure presents a schematic draw of the proposed experimental system.

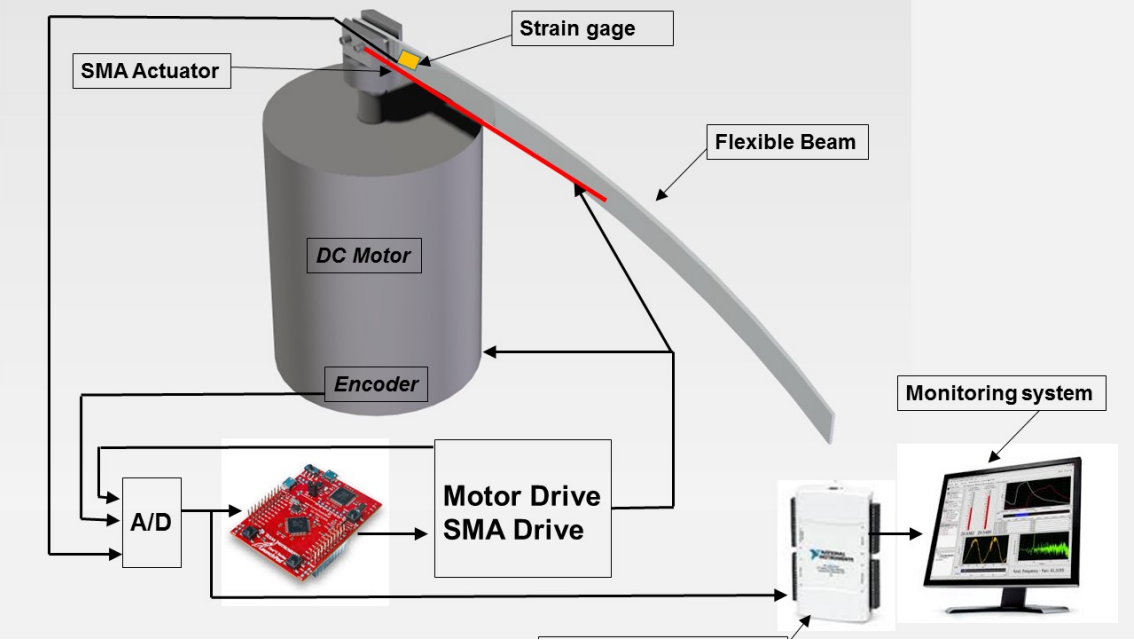

Figure 5.1: Schematic of the experimental set-up for the slewing system.

The system was all instrumented in order to turn possible to control the system in closed loop, and to turn possible the data acquisition of the system variables for a further analysis.

The instrumentation are compose of various sensors, like as current sensors and angular position sensors. The variables of the system which are important to be measured are: the first vibration mode displacement, the angular position of the DC motor shaft, the current applied to the DC motor terminals and the current applied to the SMA actuator.

To measure the beam displacement due the vibration, one pair of strain gage sensor mounted in a half bridge configuration are applied to the aluminium beam near to its fixed end, where it is easier to measure the first vibration mode. Figure 5.2, presents a schematic draw of the strain gage assembly in the half bridge configuration.

To measure the angular position of the DC motor shaft, a magnetic field encoder is applied. The great advantage of this kind of sensor is that it does not have a mechanical coupling with the motor shaft, which is important because it do not have any kind of friction. The angular position measure is made through a magnetic field sensor. The sensor applied in this work is the AS5145 (Fig. 5.3) produced by Austria Micro Systems.

This sensor have a resolution of 4096 bits per revolution, which means that the minimum angle displacement that can be measured is 0.087°. Other advantage is the low noise of the measured signal because the sensor transmits the data in a digital serial form.

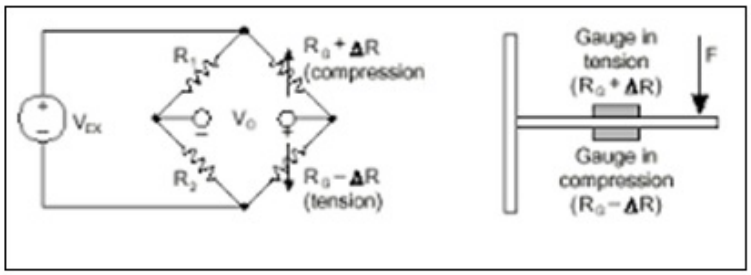

Figure 5.2: Schematic illustration of the strain gage sensor in half bridge configuration.

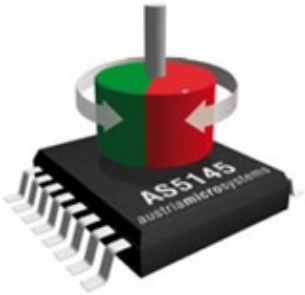

Figure 5.3: Magnetic field encoder applied to measure the angular position of the motor shaft (System, 2010).

For the current measurement applied to the DC motor and SMA actuator, a hall-effect current sensor is applied. The chosen sensor for this work is the ACS712, which can measure currents at list 30 Amps with a resolution 0.185 Volt/Amp.

In order to drive the DC motor a driver circuit need to be used. This circuit is used to convert the control signal, generated by a microcontroller, to a higher power signal, which can supply the DC motor, and to invert the current signal. The development of this circuit is presented in section 5.2.

The SMA actuation circuit is composed only of a BD 139 transistor, which is switched to apply the current to the SMA wire.

To control the slewing system, a TM4C123G microcontroller is used. This microcontroller is responsible to control the angular position by controlling the current applied to the DC motor, and to control the SMA activation. Figure 5.4 presents an image of the microcontroller.

In order to save the data generated by system, a data acquisition system composed of a data acquisition board NI USB-6212 connected to a software written in the LabView programming language. The data of al sensors are saved in order to analyse the system behaviour.

Figure 5.5 presents an image of the experimental slewing system.

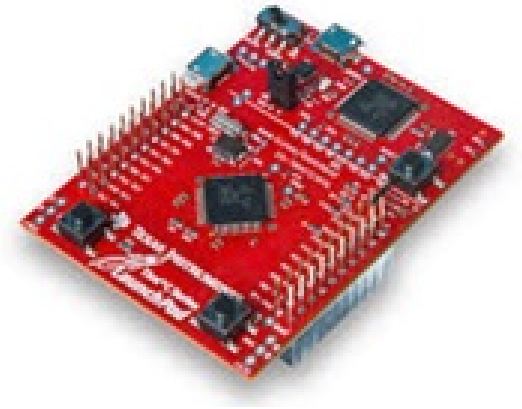

Figure 5.4: TM4C123G development pad (instruments, 2013).

Figure 5.5: Image of the experimental set-up of the slewing system.

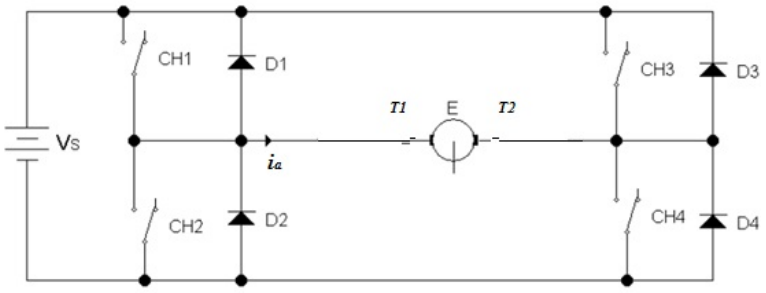

Figure 5.6: Schematic of the proposed motor drive.

In Fig. 5.5 it is possible to see the power sources, the DC motor driver circuit, right side, and in the left side the slewing system.

5.2 Motor Drive development

This section will present the methodology of selection and development of the DC motor drive circuit. This drive circuit also known as chopper or DC-DC converter, is necessary for the system to be responsible for controlling the power delivered to the load (DC motor). In this sense, it is necessary that the drive circuit respect two design requirements in order to suit the system proposed in the section 5.1.

The first requirement relates to chopper topology, which must allow the reversion of motor rotating direction, in order to control the angular position of the flexible structure. This requires that the chopper allow the inversion of the supply polarity applied to the motor terminals.

The second condition refers to the power supplied to the DC motor. The chopper should supply the system with a supply voltage up until 12 Volts and support a peak current of up to 10 Amps. The same should also be able to control the power delivered to the output load as required by the controller.

The selection of appropriate driving circuit also depends on the DC motor operation, which can be divided in the form of quadrants as shown by (Patané, 2008).

In the first quadrant, the speed and the motor torque are positive, whereas it undergoes a positive acceleration. In the second quadrant, the speed is negative and the torque is positive, and the motor decelerates. The three and four-quadrant has the same functioning of quadrants one and two respectively, but with an inverted rotation direction.

Rashid (2009) classifies the DC-DC converters in five operating classes which are named by the letters A to E. The drive selected for this project is the E class, which is a four-quadrant converter, and the only one that respect all the requirements for the project. A schematic diagram of the converter is shown in Fig. 5.6.

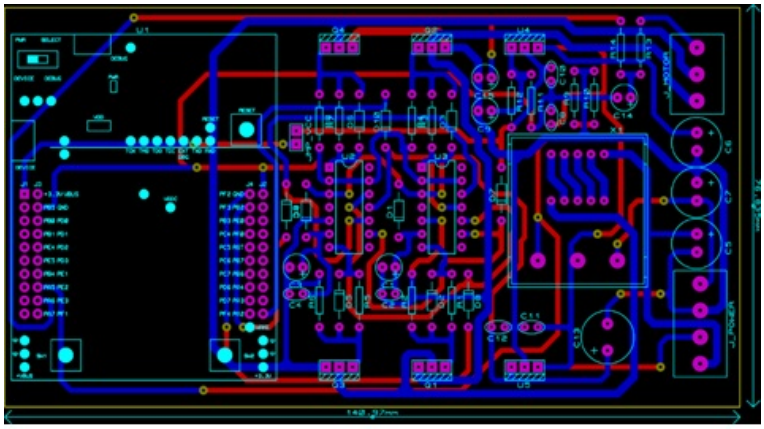

Figure 5.7: Image of the developed circuit for the DC motor drive.

When the switches CH1 and CH4 are closed, the supply current passes in the direction from T1 to T2 (DC motor terminals), causing a torque motor in the positive direction. When the switches CH3 and CH2 are closed the current direction over T1 to T2 inverts its direction from T2 to T1, and the torque generated by the motor is negative. To control the power of the load, it uses a PWM control signal (Pulse Width Modulation) applied to the switches.

The function of the diodes D1 to D4 is to prevent that short circuits occurs due to the induced currents by the motor over the switches, which in this project are power MOSFET's IRF640. This MOSFET type is designed to work in high frequency's with high current capacity, and is compatible with the design requirements.

It is important to pay attention that the CH1 and CH2, CH3 and CH4 never should be pressed simultaneously, which can cause a short circuit of the source. To avoid this problem the developed converter has a Drive IR2111 to drive the switches. This drive is responsible for receiving the microcontroller control signals and switch the system efficiently.

After selection and drive circuit design for the DC motor, it was developed and assembled. Appendix B shows the image of the developed electronic circuit, and Fig. 5.7 shows the layout of the designed circuit. After prototype the phenolite plate and the welded components in their respective positions the result obtained is shown in Fig. 5.7.

Figure 5.8, presents an image of the developed DC motor drive.

It is important to point out that the dynamics of the DC motor drive is not considered in the model proposed in chapter 2. This model simplification is due the increasing complexity of the model when the dynamics of the motor drive is considered.

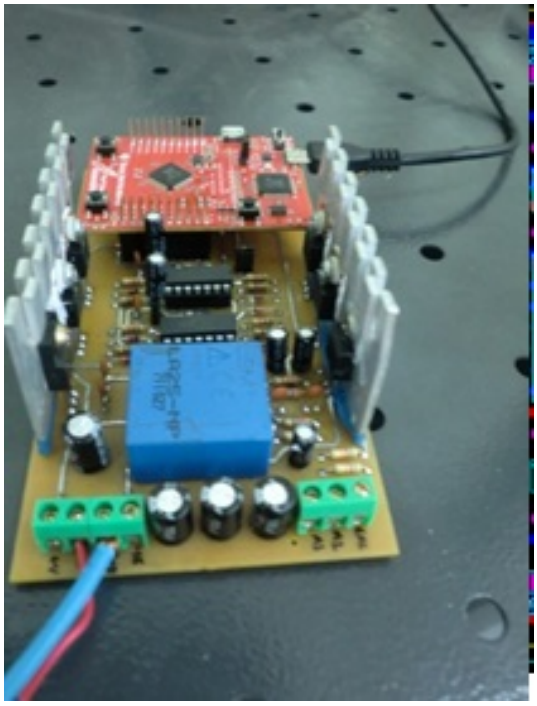

Figure 5.8: Image of the developed circuit for the DC motor drive.

5.3 Experimental results for the angular positioning control

To validate the positioning controller an experiment was performed. The experiment consist of control the angular position of the DC motor and lead it to the desired position. The desired position is localized at 1 rad. The SDRE controller was written in LabView and embedded into the microcontroller.

Figure 5.9, presents the electric current applied to the DC motor in order to position the system to the desired position.

In order to analyse the current, Fig. 5.10 presents a zoom of Fig. 5.9. The selected zoom region is the current peak between 0 and 1 seconds.

It is possible to see in Fig. 5.10, that the behaviour of the simulated system and experimental test are very close to each other. This can be assumed by comparing Fig. 5.10 with Fig. 4.2. The first peak is due the displacement start, because the motor needs to overcome the inertia. The other peaks occurs due the vibration of the beam, which is coupled to the motor shaft.

In Fig. 5.11, it is possible to see the angular position of the DC motor, for the proposed control.

By analysing the Fig. 5.11, it is possible to see that the system reaches the desired position at about 2 seconds. A overshoot can be seen, which can be explained due the

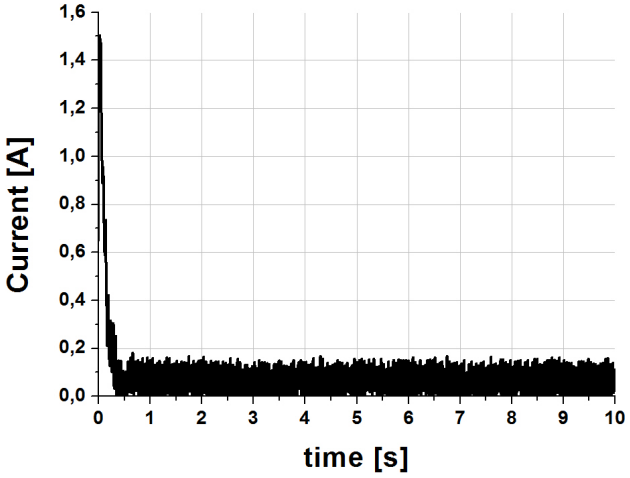

Figure 5.9: Measured DC motor current for the positioning control.

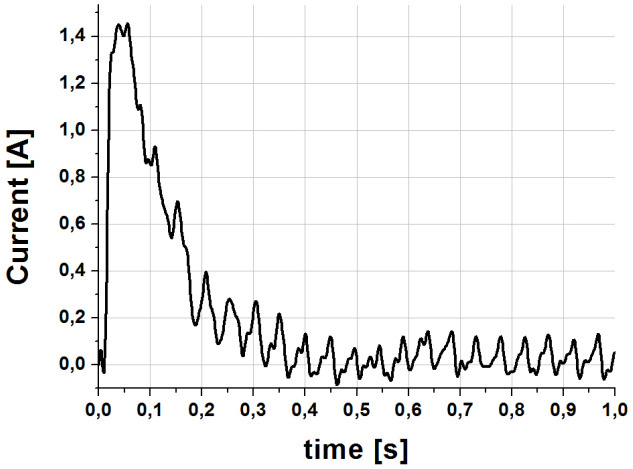

Figure 5.10: Zoom of the electric current signal presented in Fig. 5.9

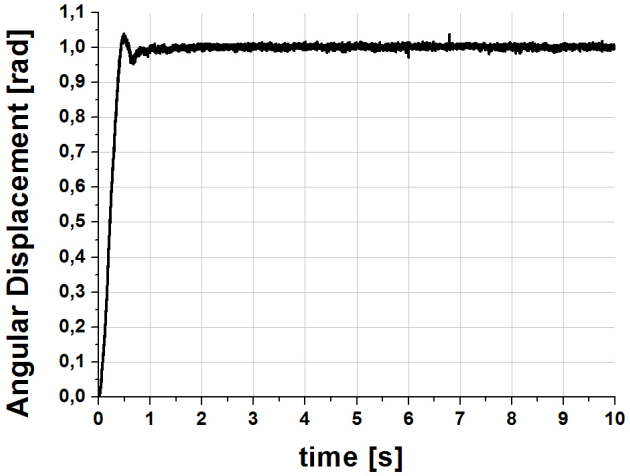

Figure 5.11: Measured angular displacement for a 1 rad desired position.

non-linearity of the DC motor, like the dead zone and coulomb friction. The dead zone is a region of voltage for which the DC motor does not responds to the controller.

Figure 5.12, shows the displacement of the beam free end due the vibration.

The signal of the beam displacement presented in Fig. 5.12, considers all the vibration modes. This vibration is due the DC motor positioning control. The beam displacement presented in Fig. 5.12, do not consider the SMA activation, but the SMA wire is coupled to the beam during the test.

5.4 Experimental results for the positioning and vibration control

To validate the vibration control an experimental test was performed. This tests considers the positioning control as presented in section 5.3 and the SMA actuator in order to control the vibration of the flexible beam. The SDRE controller which controls the angular positioning, and the Proportional controller, which controls the vibration are written in LabView and embedded to the microcontroller.

Figure 5.13, present the electric current applied to DC motor in order to control the system position.

In order to analyse the current, Fig. 5.14 presents a zoom of Fig. 5.13. The selected zoom region is the current peak between 0 and 1 seconds.

By analysing the electric current applied to the DC motor for the system with the SMA actuation (Fig. 5.14), and comparing it to the simulation results and to the current showed in Fig. 5.10, it is possible to see that they have the same behavior and there is

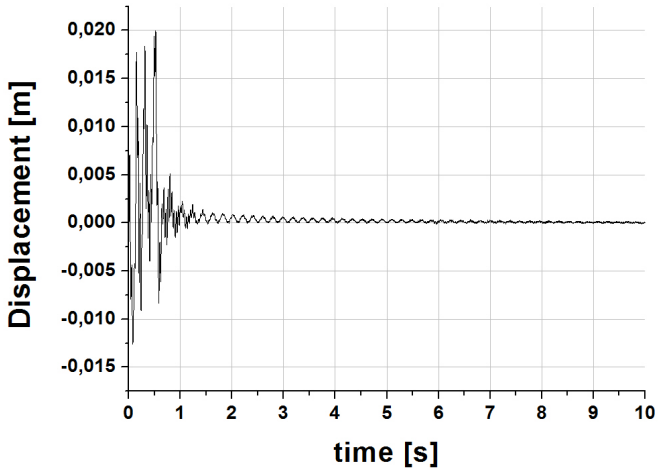

Figure 5.12: Measured beam displacement due the angular position displacement.

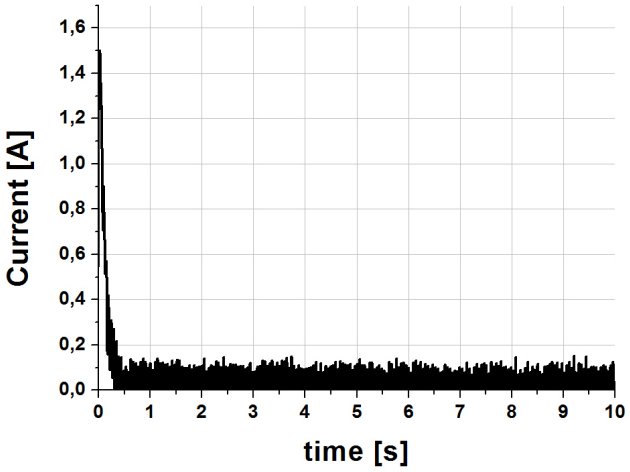

Figure 5.13: Measured DC motor current for the system with positioning control and vibration control.

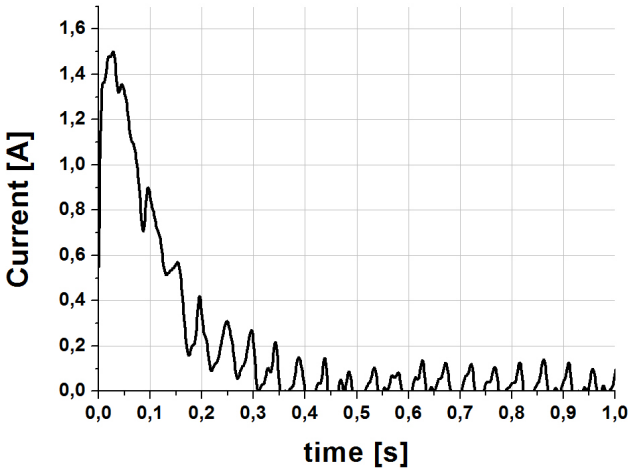

Figure 5.14: Zoom of the electric current signal presented in figure 5.13.

not a considerable difference between them. So, it is possible to assume that the SMA actuator do not have a visible influence over the current applied to the DC motor, which means that it do not have a great influence over the DC motor angular positioning, as presented in Fig. 5.15 and Fig. 5.16.

Figure 5.15, presents the angular position displacement of the DC motor shaft for the system with the SMA actuation.

It is possible to see that the SDRE control lead the system to the desired position, but presenting an overshoot signal. This overshoot can be explained by the non-linearity's like the dead zone, which is not considered in the controller project.

In Fig. 5.16, a comparison between the signals of the angular position of the DC motor for both cases (with and without SMA actuator) are compared. The both test uses the same SDRE control gains. This comparison is made in order to analyse the influence of the SMA over angular positioning of the DC motor.

By analysing Fig. 5.16, it is possible to see that there are not significant differences between the two signals. They present the same behaviour and are very close to each other. So, it is possible to affirm that the SMA actuator do not influences the DC motor control. It is possible to see that the SDRE is robust in order to control the position of the DC motor.

Figure 5.17, presents the beam displacement signal for the system with vibration control.

It is possible to see by analysing Fig. 5.17, and comparing it to Fig. 5.12, that the SMA actuator when exited, influences the beam displacement. Because of the application of the SMA actuator only in one of the beam sides, it is possible to see that when it is actuated,

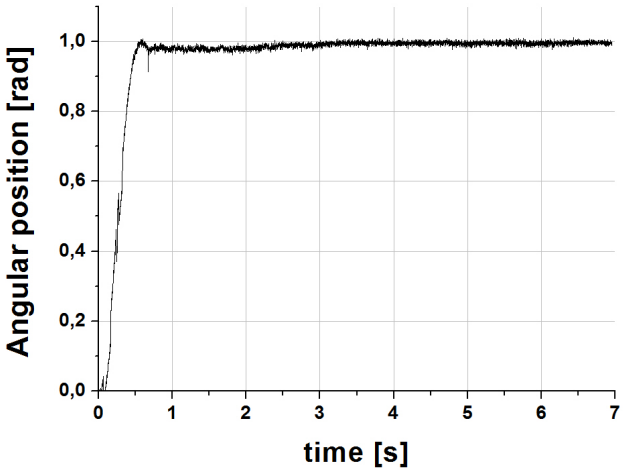

Figure 5.15: Measured angular displacement for a 1 rad desired position by considering the vibration control.

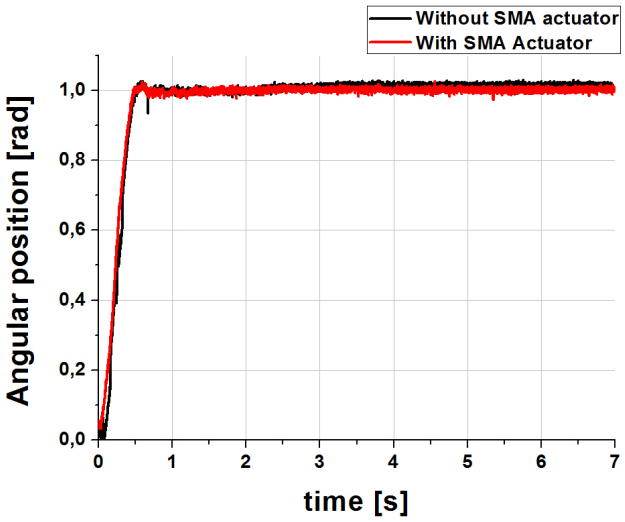

Figure 5.16: Comparison between the angular position control for the system with the SMA and without SMA actuation.

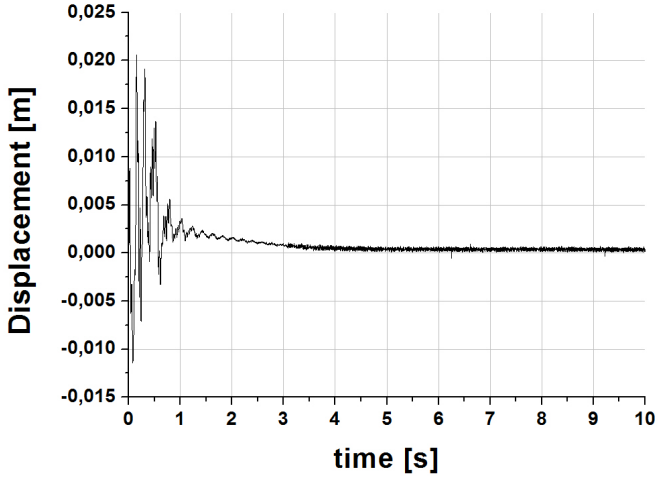

Figure 5.17: Measured beam displacement due the angular position control and SMA actuator control.

the beam deflect to the SMA side. The stress caused due the reverse phase transformation, pulls the beam the actuator side. In addition, when the forward transformation occurs, the beam turns to the original position.

Figure 5.18, presents a comparison between both beam displacement signals (with and without vibration control.

By analysing Fig. 5.18, it can be seen the influence what the SMA actuation haves over the beam displacement. The red line, presents the signal with the SMA actuation, and the black line is the beam displacement without the vibration control. It is possible to see that the SMA actuator when exited, reduces the vibration amplitude, when the phase transformation occurs. By analysing Fig. 5.18 between 0.5 and 1 seconds, it is possible to see a considerable reduction in the beam vibration amplitude.

In Fig. 5.19, a zoom of the SMA actuation region is presented.

By analysing more closely the actuation region presented in Fig. 5.19, it is possible to see the amplitude reduction in the beam displacement at 0.5 seconds. The deflection to the actuator side, due to sequential actuation can be seen to. In order to analyse the settling time, both system reach the steady state at the same time, but it is possible to see that the system with SMA actuation has less vibrations. The delay in this case is caused by the forward transformation, which occurs due natural convection and have a higher time as the reverse transformation, which pulls the system to the SMA actuator side.

Figure 5.20, presents the control signal applied to the SMA actuator.

By comparing the simulated signal (Fig. 4.12) whit the experimental control signal (Fig. 5.20), it is possible to see a significant difference. This difference can be explained because the experimental signal is applied in the PWM form, and the simulated signal is

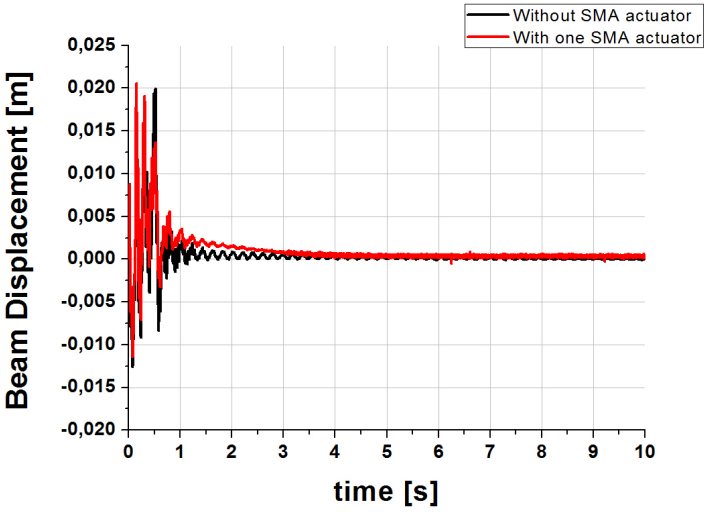

Figure 5.18: Comparison between the beam vibration for the system with the SMA actuation (in red), and without the SMA actuation (in black).

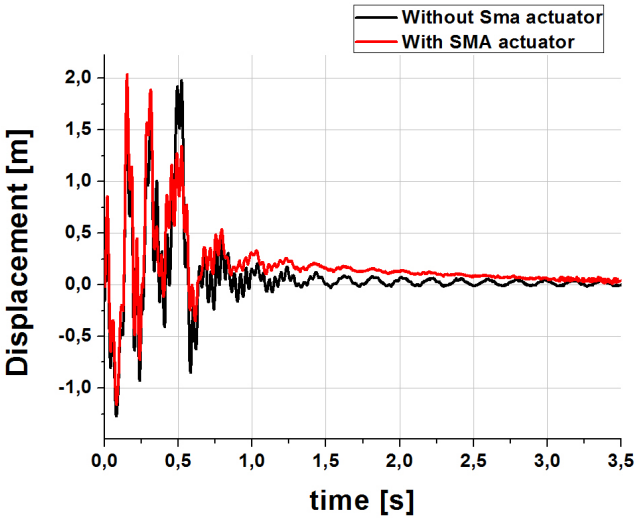

Figure 5.19: Zoom of the beam displacement comparison in figure 5.18.

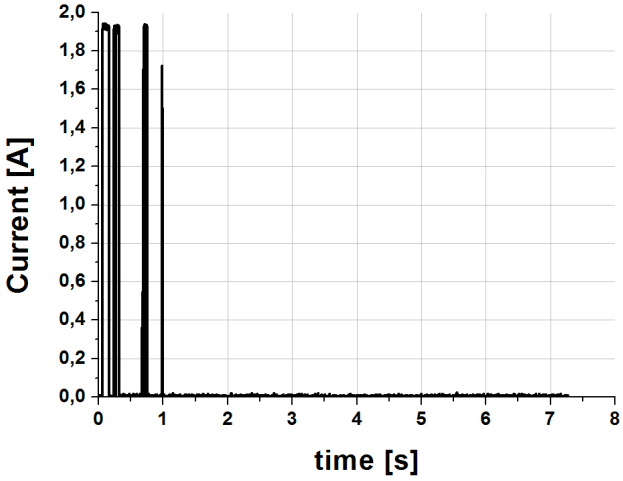

Figure 5.20: Measured current applied to the SMA actuator for the vibration control.

the direct proportional signal. By analysing the SMA control signal it is possible to see a close behaviour to the simulated signal.

Chapter 6

Conclusions

Flexible structures in slewing motion are encountered in many kinds of applications, so the importance of their study. They are much lighter than its rigid concurrent, which makes it possible to work in space for example. The flexibility brings a big challenge in order to control the system due the higher vibration amplitudes of the flexible structures. This vibrations are coupled to the system and interfere in its normal work, therefore they can not be overlooked.

This work have proposed the application of Shape Memory Alloys actuators applied to the flexible structure to control the vibrations. The SMA's are a metallic alloy which have the capacity to return to its original shape after they are deformed. The great advantage of this kind of material is its high actuation force per volume ration. This capacity is the reason of the application of these materials in this thesis. This turns possible to control the vibration of a flexible structure without increase significantly the system mass. Other advantage of the SMA actuator is its low actuation power which is an important variable to take account today where the systems need to be very time more efficient.

This work have demonstrate the modeling of a DC motor and its numerical simulations compared to the experimental results have demonstrate the proposed mathematical model represents very closely the dynamic behavior of the real motor, thus demonstrate that the model can be used to represent the DC motor in numerical simulations of systems such as it presented in this thesis.

Important results was obtained by analyzing the effects of the coupling of the DC motor to a beam like structure. This results showed that for high rotation speeds the air drag force need to be considered into the model because of its effect over the motor torque. It was showed through experimental results that the drag force increases significantly the DC motor current in higher rotation speeds.

This work have presented the application of the SDRE control technique, which was applied to control the angular positioning of the slewing system. This controller have

demonstrate its robustness in the positioning control. The results have showed that the beam vibrations which are coupled to the DC motor shaft do not interfere in the positioning time. The experimental results have demonstrate that the addition of the SMA actuator do not interfere in the positioning control.

A mathematical model for the SMA actuator was proposed. The numerical results have showed the hysteretic behavior of this kind of actuator. The experimental results have presented a similar behavior of the numerical simulations. The activation time have demonstrate to be dependent of the electric power applied to the actuator. The grate disadvantage demonstrated was the relaxation time of the actuator, which depends of the natural convection of the temperature. This behavior limits the actuation frequency of the SMA. Some works have proposed cooling methods, but they increases the system complexity and increases the system mass.

Even considering the differences between the simulation and experimental results of the SMA actuator, the presented model can be considered usable in the numerical analyses of system composed by SMA actuators. This because both results presents the same behavior.

A mathematical model for the coupling of SMA actuator and slewing flexible structure have been proposed. The numerical and experimental results have demonstrate the influence of the structure vibrations over the DC motor. The results demonstrate that the simulations experimental tests for the DC motor current have a very close behavior in relation to the vibrations which are coupled to the DC motor. This is an important affirmation because its validate the nonideal coupling of the model.

The SDRE controller have demonstrate to be efficient in order to position the system. However, in order to control the vibration of the flexible structure they demonstrate to have some difficulties. This happens because some nonlinearitys that appears for low voltages applied to the DC motor, which limits its control.

To control the vibration, a proportional controller was proposed, which works through the electric current applied to the SMA. The results have showed the complexity to control the SMA actuator due its hysteretic behavior.

The analysis of the experimental results for the system with and without the vibration control, have demonstrated that the SMA actuator can reduce significantly the vibration amplitude. This work have applied only one actuator. The results have demonstrate that the high time of the relaxation of the SMA actuator pulls the system to the SMA actuator side. Some works have proposed the use of antagonistic actuators, which can improve the presented results.

It is possible to conclude through this work that the SMA actuators are a promising actuator class for the development of more efficient systems. The models proposed have

demonstrate is capacity to reproduce the system behavior, which can be considered in order analyze with more details the system behavior or for test other control techniques for example.

Chapter 7

Future Works

This research can be continued in several directions like:

- The inclusion of the electronic drive dynamics to the system equations of motion.
- The analysis of the slewing system in high speed rotations.
- The control of the SMA actuator through more efficient control methods.
- The analysis of the effect of the SMA actuator over other vibration modes.
- The analysis of the effect of the SMA actuator over torsional vibrations.

Bibliography

Banks, H., Lewis, B., and Tran, H. (2007). Nonlinear feedback controllers and compensators: a state-dependent riccati equation approach. *Computational Optimization and Applications*, 37(2):177–218.

Brinson, L. C. (1993). One-dimensional constitutive behavior of shape memory alloys: thermomechanical derivation with non-constant material functions and redefined martensite internal variable. *Journal of intelligent material systems and structures*, 4(2):229–242.

Dorf, R. C. and Bishop, R. H. (2001). *Sistemas de controle modernos*. Livros Técnicos e Científicos.

Elahinia, M. (2004). Effect of system dynamics on shape memory alloy behavior and control.

Elahinia, M. H. and Ashrafiuon, H. (2002). Nonlinear control of a shape memory alloy actuated manipulator. *Journal of vibration and acoustics*, 124(4):566–575.

Fenili, A. (2000). Modelagem matemática e análise dos comportamentos ideal e não ideal de estruturas flexíveis de rastreamento e aplicações em engenharia mecânica. *Unicamp SP: Brasil*.

Fenili, A. and Balthazar, J. M. (2005). Some remarks on nonlinear vibrations of ideal and nonideal slewing flexible structures. *Journal of sound and vibration*, 282(1):543–552.

Fenili, A., Balthazar, J. M., and Brasil, R. (2003). Mathematical modelling of a beam-like flexible structure in slewing motion assuming non-linear curvature. *Journal of sound and vibration*, 268(4):825–838.

Gantmakher, F. R. (1970). *Lectures in analytical mechanics*. Mir publishers.

Garcia, E. and Inman, D. J. (1990a). Advantages of slewing an active structure. *Journal of Intelligent Material Systems and Structures*, 1(3):261–272.

Garcia, E. and Inman, D. J. (1990b). Modeling of actuator-structure interaction in the slewing of flexible structures. In *American Control Conference, 1990*, pages 1962–1967. IEEE.

Ge, S. S., Tee, K. P., Vahhi, I. E., and Tay, F. E. (2006). Tracking and vibration control of flexible robots using shape memory alloys. *IEEE/ASME Transactions On Mechatronics*, 11(6):690–698.

instruments, T. (2013). *Tiva C Series TM4C123G Lounchpad Evalution Board User Guide*.

Janzen, F., Tusset, A., Piccirillo, V., Balthazar, J., and Brasil, R. (2015). Motion and vibration control of a slewing flexible structure by sma actuators and parameter sensitivity analysis. *The European Physical Journal Special Topics*, 224(14-15):3041–3054.

Janzen, F. C., Tusset, Â. M., Piccirillo, V., Balthazar, J. M., de Pontes, B. R., Silveira, M., and Brasil, R. M. (2014a). Control of slewing motions of flexible structures using shape memory alloy. In *ASME 2014 International Mechanical Engineering Congress and Exposition*, pages V04BT04A028–V04BT04A028. American Society of Mechanical Engineers.

Janzen, F. C., Tusset, Â. M., Piccirillo, V., Balthazar, J. M., de Pontes, B. R., Silveira, M., and Brasil, R. M. (2014b). Controle do movimento de rastreamento de uma estrutura flexivel sujeita a amortecimento viscoso. In *CONEN 2014 Congresso Nacional de Engenharia Mecanica*, pages 1–7. ABCM.

Lagoudas, D. (2008). Shape memory alloys: Modeling and engineering applications.

Liang, C. and Rogers, C. A. (1990). One-dimensional thermomechanical constitutive relations for shape memory materials. *Journal of intelligent material systems and structures*, 1(2):207–234.

Mavroidis, C. (2002). Development of advanced actuators using shape memory alloys and electrorheological fluids. *Journal of Research in Nondestructive Evaluation*, 14(1):1–32.

Meirovitch, L. (1967). *Analytical methods in vibration*, volume 16. Macmillan, New York.

Molter, A., Da Silveira, O. A. A., Fonseca, J. S. O., and Bottega, V. (2011). Simultaneous piezoelectric actuator and sensor placement optimization and control design of manipulators with flexible links using sdre method. *Mathematical Problems in Engineering*, 2010.

Mracek, C. P. and Cloutier, J. R. (1998). Control designs for the nonlinear benchmark problem via the state-dependent riccati equation method. *International Journal of robust and nonlinear control*, 8(4-5):401–433.

Oliveira, V. A., Aguiar, M. L., and de Vargas, J. B. (2005). *Sistemas de controle: aulas de laboratório*. EESC-USP.

Paiva, A. (2004). Modelagem do comportamento termomecânico das ligas com memória de forma. *Dr. Tese, PUC-Rio, Rio de Janeiro*.

Patané, E. (2008). Implementação de controle de velocidade em malha fechada para motores de corrente contínua utilizando sistema de aquisição de dados. *Escola de Engenharia Mauá*.

Piccirillo, V., Balthazar, J. M., Pontes, B. J., and Felix, J. (2009). Chaos control of a nonlinear oscillator with shape memory alloy using an optimal linear control: Part i: Ideal energy source. *Nonlinear Dynamics*, 55(1-2):139–149.

Raghavan, J., Bartkiewicz, T., Boyko, S., Kupriyanov, M., Rajapakse, N., and Yu, B. (2010). Damping, tensile, and impact properties of superelastic shape memory alloy (sma) fiber-reinforced polymer composites. *Composites Part B: Engineering*, 41(3):214–222.

Ramos, D., Mertens, J., Calleja, M., and Tamayo, J. (2007). Study of the origin of bending induced by bimetallic effect on microcantilever. *Sensors*, 7(9):1757–1765.

Rashid, M. H. (2009). *Power electronics: circuits, devices, and applications*. Pearson Education India.

Romano, R. and Tannuri, E. A. (2009). Modeling, control and experimental validation of a novel actuator based on shape memory alloys. *Mechatronics*, 19(7):1169–1177.

Sohn, J., Han, Y., Choi, S., Lee, Y., and Han, M. (2009). Vibration and position tracking control of a flexible beam using sma wire actuators. *Journal of Vibration and Control*, 15(2):263–281.

Stieber, M. E., McKay, M., Vukovich, G., and Petriu, E. (1999). Vision-based sensing and control for space robotics applications. *IEEE Transactions on Instrumentation and Measurement*, 48(4):807–812.

System, A. M. (2010). *AS5045 12 bit Programmable Magnetic Rotary Encoder User's Guide*, austria micro system edition.

Tanaka, K. (1986). A thermomechanical sketch of shape memory effect: one-dimensional tensile behavior.

Tokhi, M. and Azad, A. (1996). Collocated and non-collocated feedback control of flexible manipulator systems. *Machine vibration*, 5(3):170–178.

Tokhi, M. O. and Azad, A. K. (2008). *Flexible robot manipulators: modelling, simulation and control*, volume 68. Iet.

Tusset, A. M., Balthazar, J. M., and Felix, J. L. P. (2012). On elimination of chaotic behavior in a non-ideal portal frame structural system, using both passive and active controls. *Journal of Vibration and Control*, page 1077546311435518.

Wei, Z., Sandstroröm, R., and Miyazaki, S. (1998). Shape-memory materials and hybrid composites for smart systems: Part i shape-memory materials. *Journal of Materials Science*, 33(15):3743–3762.

Yuvaraja, M. and Senthilkumar, M. (2013). Comparative study on vibration characteristics of a flexible gfrp composite beam using sma and pzt actuators. *Procedia Engineering*, 64:571–581.

Appendix A

DC Motor Characterization Methodology

In Sec. 2.2, the dynamic model for a DC motor is proposed with to turn possible the simulation of the slewing system. With the intend to approximate the maximum as possible the model to the real system it is important to know the correct values of the parameters of Eq. (2.4) and Eq. (2.5). The parameters can be obtained through experimental measurements. In this work the methodology applied to obtain the DC motor parameters is presented in Oliveira et al. (2005).

The first step presented by Oliveira et al. (2005) consist of measure the electric resistance R of the motor armature. It is important to consider that the resistance varies conform the angular position of the motor shaft. To obtain a better result, the final value of resistance is considered to be the lower measured value. In the same angular position in which the resistance has its lowest value, the inductance L_m is measured to.

To obtain the counter electromotive constant, K_b it is considered that the motor is turned on and in steady state. In this case it is possible to affirm that the current absorbed by the motor is constant, or, $\frac{di_a}{dt} = 0$ therefore we can rewrite Eq. (2.5) as presented in Eq. (A.1).

$$K_b = \frac{V - Ri_a}{\dot{\theta}} \tag{A.1}$$

Thus, it is possible to obtain the value of K_b, being that the resistance, voltage, current, and angular speed values are easily obtained from direct measurements .

Considering the motor in steady state, the values of the static and viscous friction can be obtained by stating that $\frac{d\dot{\theta}}{dt} = 0$ and $\frac{di_a}{dt} = 0$. In this case it is possible to affirm that all the energy consumed by the DC motor is used to overcome the losses due to the friction

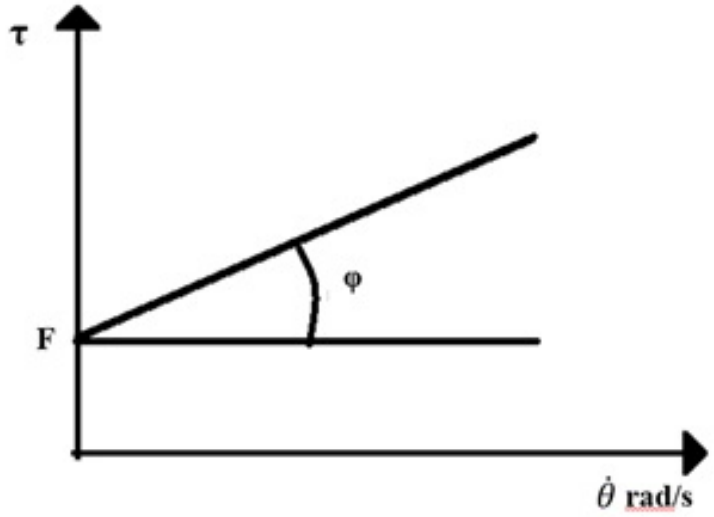

Figure A.1: Graphic representation of the relation between the generated torque and the angular speed of a DC motor.

and Joule effect. So it is possible to rewrite Eq. (2.4) as presented in Eq. (A.2)

$$b\dot{\theta} + F = K_t i_a = \tau \tag{A.2}$$

Where F is the viscous friction of the motor.

From the energetic balance of the DC motor, and considering Vi_a as the total power send to the motor, $Ri_a{}^2$ as the sum of the resistive losses, and $\tau\dot{\theta}$. as the mechanical losses, Eq. (A.3) is obtained.

$$\tau = \left(\frac{V - Ri_a}{\dot{\theta}}\right) i_a \tag{A.3}$$

All the parameters presented in Eq. (A.3) can be experimentally measured and the torque value can be easily obtained.

The graph presented in figure A.1, which presents the relation between the torque and the angular speed, can be used to obtain the static and viscous frictions.

The value of the viscous friction is obtained through the Fig. A.1 by considering that $b = \tan(\varphi)$.

The torque constant K_t normally is considered as the same numeric value of the K_b constant.

To obtain the value of the moment of inertia, J, it is considered that the motor is in steady state and the power is turned off suddenly. The moment of inertia is than obtained through Eq. (A.4).

$$J = b\dot{\theta}_{reg} \tag{A.4}$$

where $\dot{\theta}_{reg}$ represents the speed in steady state multiplied per 0.386.

Appendix B

Motor Drive Electric Schematic

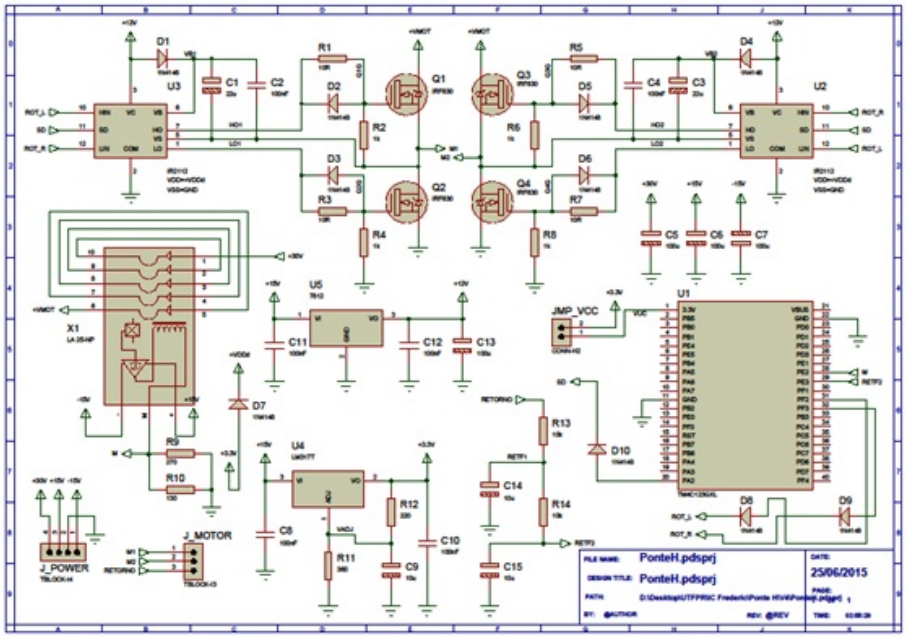

Figure B.1: Dc motor drive board electric project

Vita

Frederic Conrad Janzen was born in 28 th August, 1987, in São José dos Pinhais, PR, Brazil. He earned his technologist degree in Industrial Automation in Federal University of Technology-Paraná – Campus Ponta Grossa, Brazil, 2009. Moreover, he received his Master's degree in Electrical Engineering in the University of Technology-Paraná – Campus Curitiba, Brazil, 2012. Since than he works as Assistant professor in the University of Technology-Paraná – Campus Ponta Grossa. He joined the Ph.D. program in Mechanical Engineering in the Faculty of Mechanical Engineering of Bauru at Sao Paulo State University - Campus Bauru, Brazil, in 2nd semester of 2013. Since then, he has been working under the supervision of Full Professor José Manoel Balthazar.

During his studies in the Ph.D course, he published many articles with his supervisor and co-authors that are listed above.

1) Published articles in international journals

· **JANZEN, F.C.**, TUSSET, A.M., PICCIRILLO, V., BALTHAZAR, J.M., BRASIL, R.M.L.R.F.. Motion and vibration control of a slewing flexible structure by SMA actuators and parameter sensitivity analysis. The European Physical Journal. Special Topics, v. 224, p. 3041-3054, 2015.

· LIMA, J. J., TUSSET, A. M., **JANZEN, F. C.**, PICCIRILLO, V., NASCIMENTO, C. B., BALTHAZAR, J. M., BRASIL, M. R. L. F.. Nonlinear state estimation and control applied to a manipulator robotic including drive motor. Mathematics in Engineering, Science and Aerospace: the transdisciplinary international journal, v. 5, p. 413-425, 2014.

· TUSSET, A. M., PICCIRILLO, V., **JANZEN, F. C.** , LENZ, W. B., LIMA, J. J., BALTHAZAR, J. M., BRASIL, M. R. L. F.. Suppression of vibrations in a nonlinear half-car model using a magneto-rheological damper. Mathematics in Engineering, Science and Aerospace: the transdisciplinary international journal, v. 5, p. 427-443, 2014.

2) Articles published in international refereeing conferences

· **JANZEN, F. C.**, TUSSET, A. M., BALTHAZAR, JOSÉ MANOEL . Positioning Control of a Flexible Slewing Structure by Applying Sliding Mode Control. In: DETC -ASME 2016, 2016, Charlotte, NC, USA. Proceedings of ASME-IDETC/CIE 2016. NY, USA: ASME, 2016. v. 2016. p. 1-10.

· **JANZEN, F. C.**, TUSSET, A. M., PICCIRILLO, V., BALTHAZAR, J. M., SILVEIRA, M., PONTES JR, B.R.. Control of Slewing Motions of Flexible Structures using Shape Memory Alloy actuators. In: IMECE 2014- ASME 2014 International Mechanical Engineering Congress Exposition, 2014, Montreal. ASME, 2014, 2014. p. 1-10.

· TUSSET, ÂNGELO MARCELO, PICCIRILLO, VINÍCIUS, **JANZEN, FREDERIC CONRAD**, LENZ, WAGNER BARTH, BALTHAZAR, JOSÉ MANOEL, DA FONSECA BRASIL, REYOLANDO M. L. R.. Suppression of chaotic vibrations in a nonlinear half-car model. In: 10TH International Conference on Mathematical Problems in Engineering, Aerospace and Sciences: ICNPAA 2014, 2014, Narvik. p. 1127-1136.

· DE LIMA, JEFERSON J., TUSSET, ANGELO M., **JANZEN, FREDERIC C.**, PICCIRILLO, VINICIUS, NASCIMENTO, CLAUDINOR B., BALTHAZAR, JOSÉ M., BRASIL, REYOLANDO M. L. R. DA FONSECA . SDRE control strategy applied to a nonlinear robotic including drive motor. In: 10TH International Conference on Mathematical Problems in Engineering, Aerospace and Sciences: ICNPAA 2014, 2014, Narvik. p. 565-574.